BIMONTHLY REPORT

RESEARCH STUDY ON STABILIZATION AND CONTROL

MODERN SAMPLED-DATA CONTROL THEORY

SYSTEMS RESEARCH LABORATORY

P.O. BOX 2277, STATION A
3206 VALLEY BROOK DRIVE
CHAMPAIGN, ILLINOIS 61820

PREPARED FOR GEORGE C. MARSHALL SPACE FLIGHT CENTER

HUNTSVILLE, ALABAMA

BI-MONTHLY REPORT

RESEARCH STUDY ON STABILIZATION AND CONTROL

— MODERN SAMPLED-DATA CONTROL THEORY

SUBTITLE: STABILITY ANALYSIS OF THE LOW-COST LARGE SPACE TELESCOPE SYSTEM

May 1, 1975 NAS8-29853

BY B.C.KUO
G.SINGH

PREPARED FOR GEORGE C. MARSHALL SPACE FLIGHT CENTER

HUNTSVILLE, ALABAMA

CONTRACT NAS8-29853 DCN 1-2-40-23018

SYSTEMS RESEARCH LABORATORY

P.O. BOX 2277, STATION A
CHAMPAIGN, ILLINOIS 61820

TABLE OF CONTENTS

2. Stability of the Analog Low-Cost Large Space Telescope Due to Quantization

2-1. Introduction

The objective of this chapter is to conduct an investigation on the pointing stability of the low-cost Large Space Telescope (LST) System under the influence of quantization at various locations of the system. Only the analog model of the LST system is considered in this chapter. The stability of the digital LST system with quantization is considered in Chapters 5 and 6.

The block diagram of the simplified analog LST system with quantizers is shown in Fig. 2-1.

The describing function method is used to determine the condition of self-sustained oscillation in the LST system due to the effect of each of the three quantizers acting alone. The present analysis considers only one quantizer at a time.

Let the analog describing functions of the quantizers Q_D, Q_T, and Q_R be represented by N_D, N_T, and N_R, respectively. In general, the describing function of a quantizer nonlinearity is a function of the input amplitude, E; quantization level, h; and the number of quantization levels, n, which depends on E.

For the LST system shown in Fig. 2-1, the "characteristic equations" of the system when each one of the quantizers is acting, are given as follows:

Displacement Quantizer Q_D:

$$J_v s^3 + N_D(K_p s + K_I) + K_R s^2 = 0 \tag{2-1}$$

Torque Quantizer Q_T:

$$J_v s^3 + N_T(K_R s^2 + K_p s + K_I) = 0 \tag{2-2}$$

Rate Quantizer Q_R:

$$J_v s^3 + K_p s + K_I + N_R K_R s^2 = 0 \tag{2-3}$$

These equations can be conditioned by dividing both sides of the equations by the terms that do not contain the describing function, so that the stability equation is expressed in the form of

$$1 + NG(s) = 0 \tag{2-4}$$

where N is the describing function, and G(s) is a linear transfer function. The condition of self-sustained oscillations is found by investigating the possible intersections between the trajectories of -1/N and G(s) in the complex plane.

For the equations given in Eqs. (2-1), (2-2) and (2-3), the equivalent transfer functions are

$$G_D(s) = \frac{K_p s + K_I}{s^2(J_v s + K_R)} \tag{2-5}$$

$$G_T(s) = \frac{K_R s^2 + K_p s + K_I}{J_v s^3} \tag{2-6}$$

$$G_R(s) = \frac{K_R s^2}{J_v s^3 + K_p s + K_I} \tag{2-7}$$

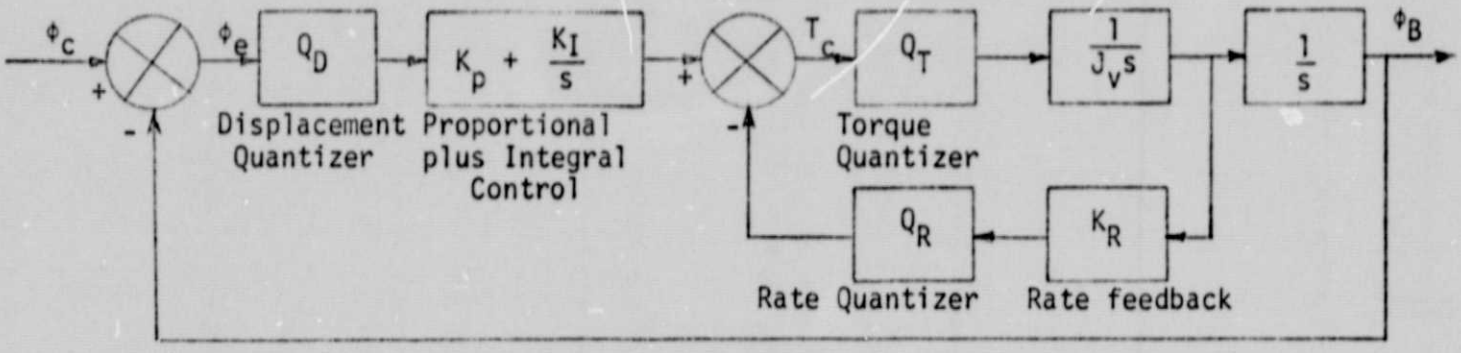

Figure 2-1. Simplified analog LST system with quantization.

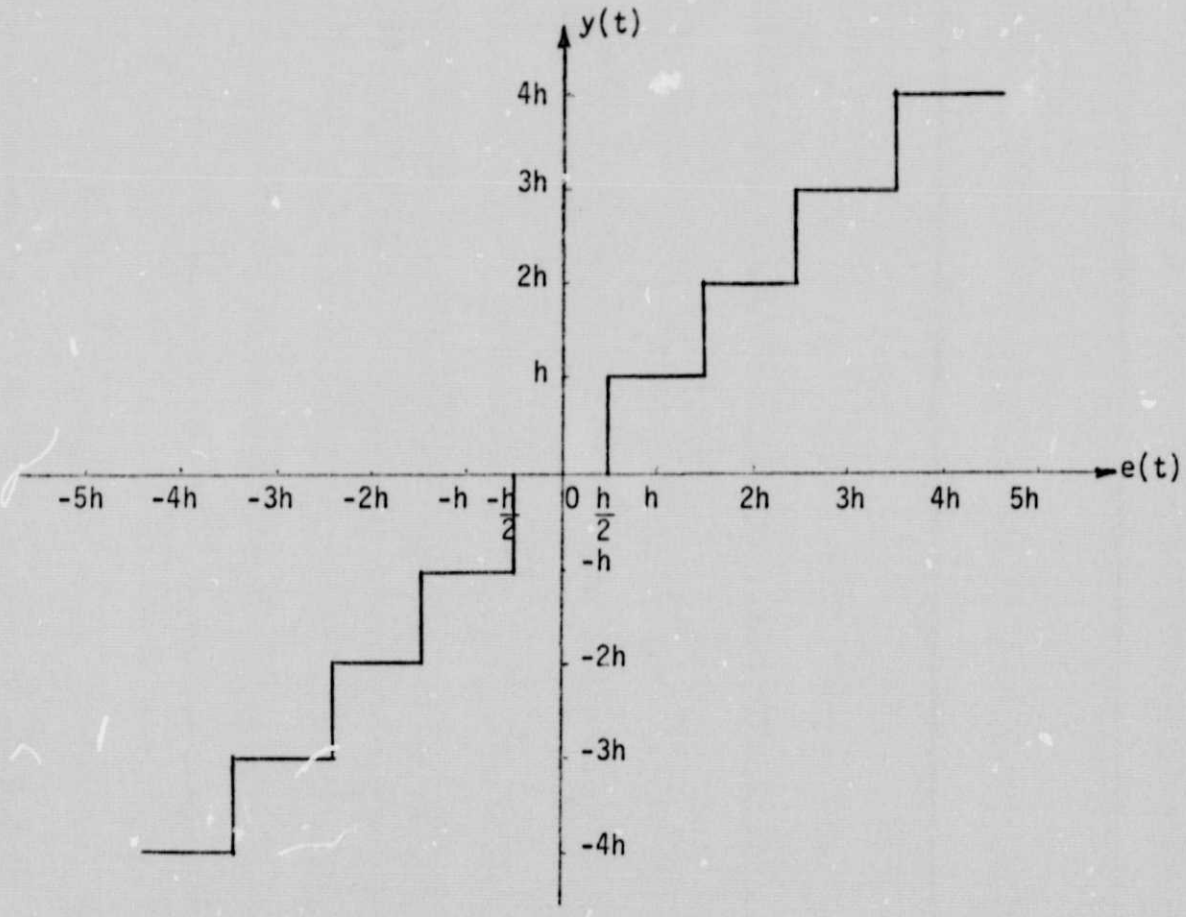

Figure 2-2. Input-output relation of a quantizer.

2-2. Analog Describing Function of the Quantizer Nonlinearity

Consider that a quantizer has the input-output relation as shown in Fig. 2-2. Let the input to the quantizer be a sine wave,

$$e(t) = E \sin \omega t \tag{2-8}$$

The quantization level is h, and let the magnitude of E be such that

$$\frac{(2n - 1)h}{2} \leq E < \frac{(2n + 1)h}{2} \tag{2-9}$$

where n is a positive integer. A typical output of the quantizer is shown in Fig. 2-3.

The fundamental component of the Fourier series expansion of y(t) is

$$y_1(t) = Y_1 \sin \omega t \tag{2-10}$$

where

$$Y_1 = \frac{4}{\pi} \int_{\alpha_1}^{\pi/2} y(t) \sin \omega t \, d\omega t \tag{2-11}$$

Evaluating the last integral, we have

$$\begin{aligned} Y_1 &= \frac{4}{\pi} \int_{\alpha_1}^{\alpha_n} y(t) \sin \omega t \, d\omega t + \frac{4}{\pi} \int_{\alpha_n}^{\pi/2} nh \sin \omega t \, d\omega t \\ &= \frac{4}{\pi} \sum_{i=1}^{n-1} \int_{\alpha_i}^{\alpha_{i+1}} ih \sin \omega t \, d\omega t + \frac{4}{\pi} \int_{\alpha_n}^{\pi/2} nh \sin \omega t \, d\omega t \end{aligned} \tag{2-12}$$

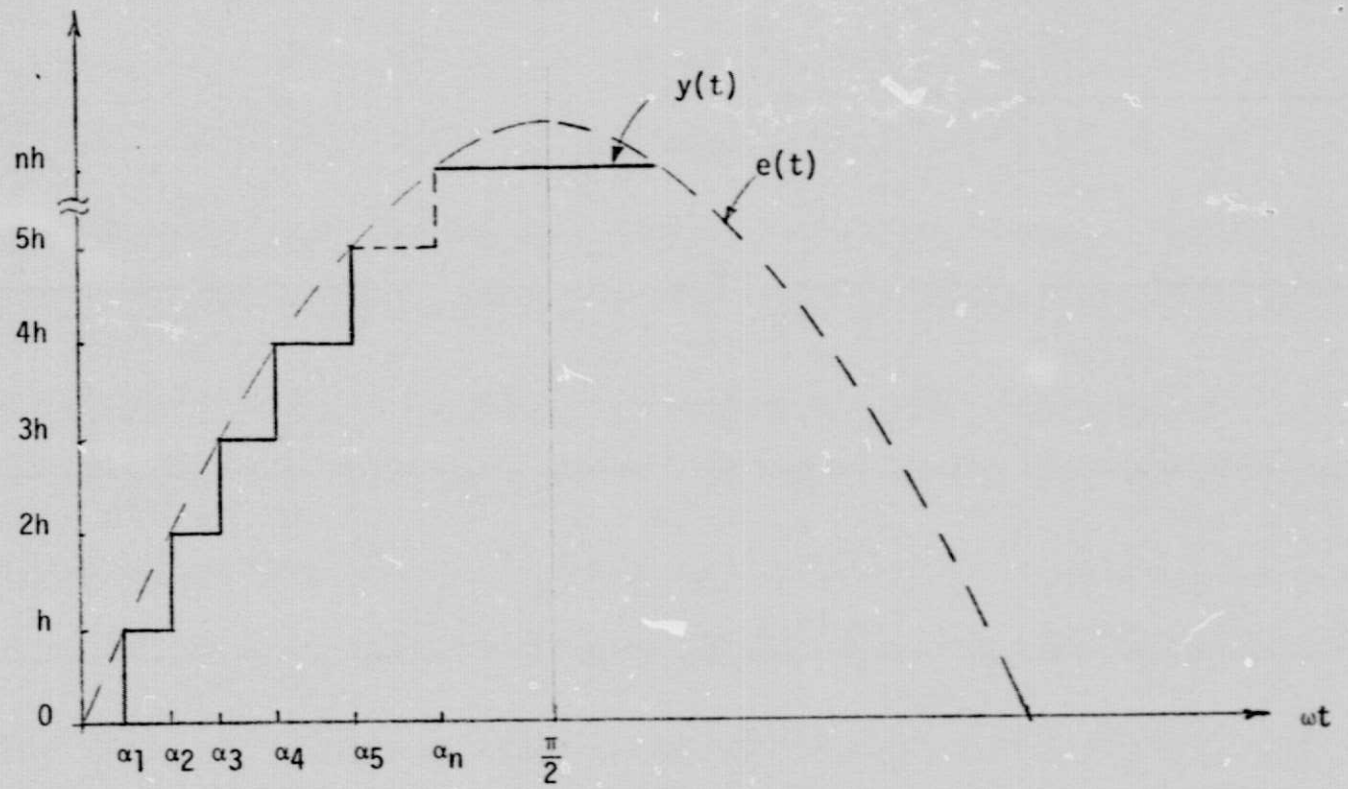

Figure 2-3. Output of a quantizer corresponding to a sinusoidal input.

Then,

$$Y_1 = -\frac{4h}{\pi}\sum_{i=1}^{n-1} i[\cos\alpha_{i+1} - \cos\alpha_i] + \frac{4nh}{\pi}\cos\alpha_n \tag{2-13}$$

Since

$$\sin\alpha_1 = \frac{h}{2E} \tag{2-14}$$

$$\sin\alpha_i = \frac{(2i-1)h}{2E} \tag{2-15}$$

$$\cos\alpha_1 = \sqrt{1 - \left(\frac{h}{2E}\right)^2} \tag{2-16}$$

$$\cos\alpha_i = \sqrt{1 - \left(\frac{(2i-1)h}{2E}\right)^2} \tag{2-17}$$

Expanding the right-hand side of Eq. (2-13), we can show that

$$Y_1 = \frac{4h}{\pi}\sum_{i=1}^{n}\cos\alpha_i \tag{2-18}$$

Substituting Eq. (2-17) into Eq. (2-18), we have

$$Y_1 = \frac{4h}{\pi}\sum_{i=1}^{n}\left\{1 - \left[\frac{(2i-1)h}{2E}\right]^2\right\}^{1/2} \tag{2-19}$$

The describing function of the quantizer is written as

$$N(E/h) = \frac{Y_1}{E} = \frac{4h}{\pi E}\sum_{i=1}^{n}\left\{1 - \left[\frac{(2i-1)h}{2E}\right]^2\right\}^{1/2} \tag{2-20}$$

Figure 2-4 shows the plot of N(E/h) as a function of E/h. We shall show in the following that

$$\lim_{\frac{E}{h}\to\infty} N(E/h) = 1 \tag{2-21}$$

Letting $\chi = E/h$, Eq. (2-20) is written

$$N(\chi) = \frac{4}{\pi\chi} \sum_{i=1}^{n} \left\{1 - \left[\frac{2i - 1}{2\chi}\right]^2\right\}^{1/2} \tag{2-22}$$

Expanding the quantity inside the summation sign in the last equation, we have

$$N(\chi) = \frac{4}{\pi\chi} \sum_{i=1}^{n} \left\{1 - \frac{1}{2}\left(\frac{i}{\chi} - \frac{1}{2\chi}\right)^2 - \frac{1}{8}\left(\frac{i}{\chi} - \frac{1}{2\chi}\right)^4 - \frac{3}{48}\left(\frac{i}{\chi} - \frac{1}{2\chi}\right)^6 - \frac{15}{384}\left(\frac{i}{\chi} - \frac{1}{2\chi}\right)^8 - \cdots\right\} \tag{2-23}$$

Or

$$N(\chi) = \frac{4}{\pi\chi} \sum_{i=1}^{n} \left\{1 - \frac{1}{2\chi^2}\left(i - \frac{1}{2}\right)^2 - \frac{1}{8\chi^4}\left(i - \frac{1}{2}\right)^4 - \frac{3}{48\chi^6}\left(i - \frac{1}{2}\right)^6 - \frac{15}{384\chi^8}\left(i - \frac{1}{2}\right)^8 - \cdots\right\} \tag{2-24}$$

Taking limit as χ approaches infinity and n approaches infinity, in the last equation, we get

$$\lim_{\substack{X\to\infty \\ n\to\infty}} N(X) = \lim_{\substack{X\to\infty \\ n\to\infty}} \frac{4}{\pi X} \sum_{i=1}^{n} \left[1 - \frac{i^2}{2X^2} - \frac{i^4}{8X^4} - \frac{3i^6}{48X^6} - \frac{15i^8}{384X^8} - \cdots \right]$$

$$= \lim_{\substack{X\to\infty \\ n\to\infty}} \frac{4}{\pi X} \left[n - \frac{1}{2X^2}\frac{n^3}{3} - \frac{1}{8X^4}\frac{n^5}{5} - \frac{3}{48X^6}\frac{n^7}{7} - \frac{15}{384X^8}\frac{n^9}{9} - \cdots \right]$$

$$= \frac{4}{\pi} \left[1 - \frac{1}{2}\frac{1}{3} - \frac{1}{8}\frac{1}{5} - \frac{3}{48}\frac{1}{7} - \frac{15}{384}\frac{1}{9} - \cdots \right]$$

$$= \frac{4}{\pi} \int_0^1 \sqrt{1 - X^2}\, dX$$

$$= \frac{4}{\pi} \left[X\sqrt{1 - X^2} + \frac{1}{2} \sin^{-1} X \right]_0^1$$

$$= 1 \qquad (2\text{-}25)$$

Since the describing function of the quantizer nonlinearity is always a real number, the function -1/N(E/h) in the magnitude (db) versus phase coordinates will lie on the -180-degree axis for all values of E/h. The plot in Fig. 2-4 shows that the magnitude of -1/N(E/h) is infinite for $0 \leq E/h < 0.5$. For $0.5 \leq E/h \leq 0.707$, the plot of -1/N(E/h) extends from infinity to -2.09 db along the -180-degree axis. Over the range of $0.707 \leq E/h \leq 1.5$, -1/N(E/h) extends from -2.09 db to 1.9 db along the -180-degree axis, etc. As E/h approaches infinity, the plot of -1/N(E/h) is reduced to the zero-db point. Figure 2-5 shows the plot of N(E/h) in magnitude versus E/h and shows the multivalued property of the function.

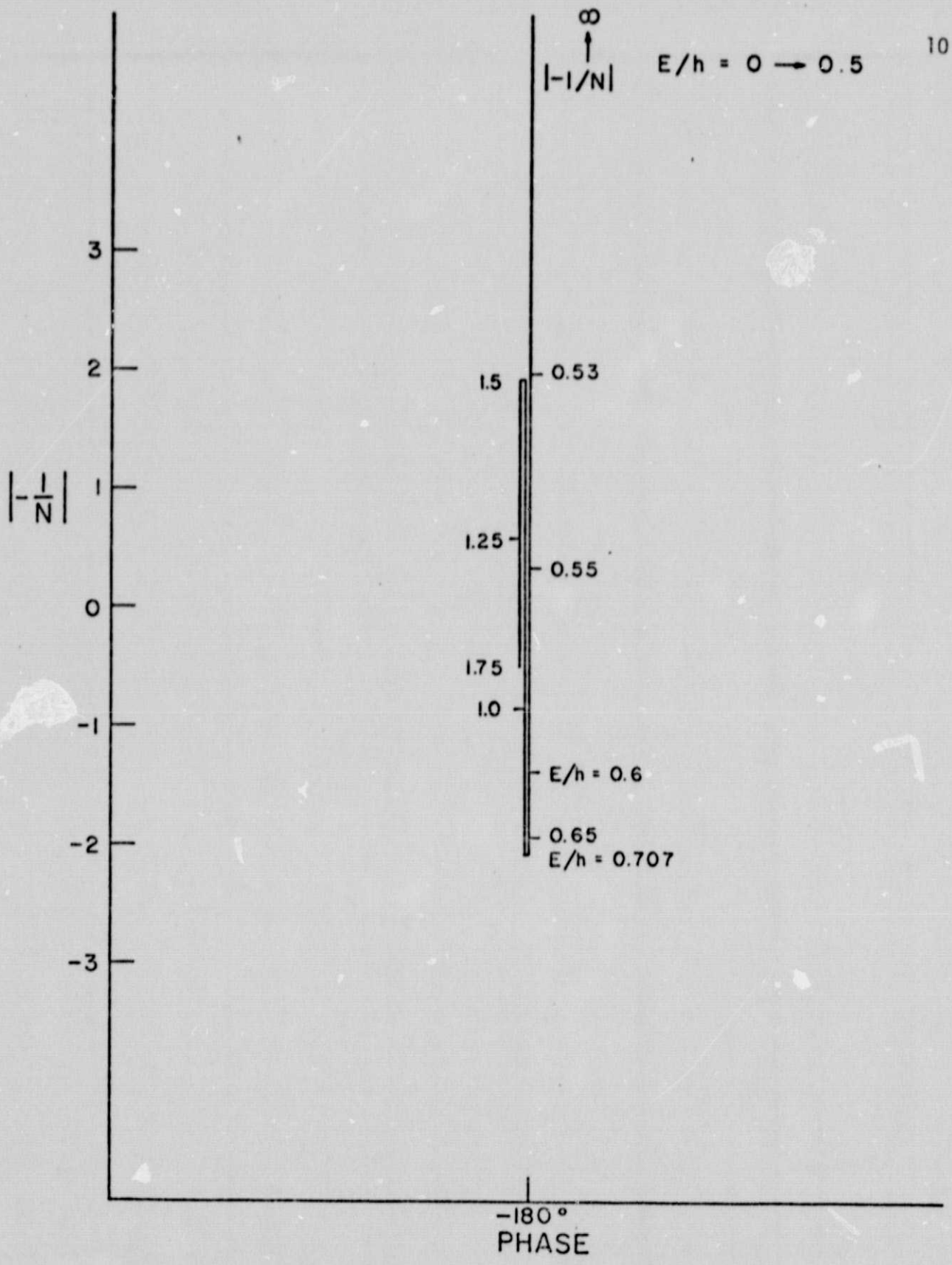

Figure 2-4. Analog describing function for the quantizer nonlinearity.

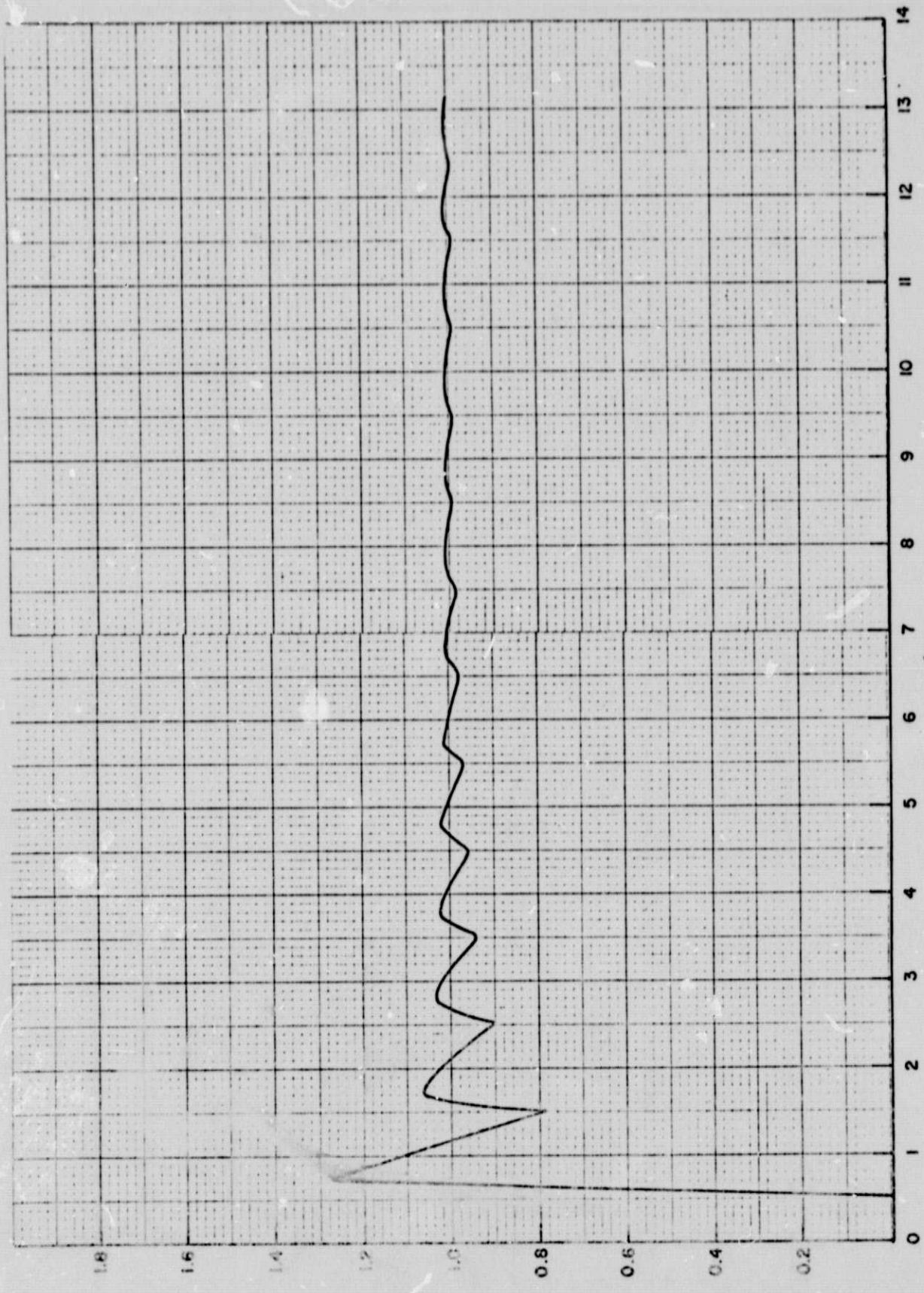

Figure 2-5. Describing function plot for the quantizer nonlinearity.

2-3. Self-Sustained Oscillations of the Analog LST System with Quantization

The transfer functions of the three quantizers, Q_D, Q_T, and Q_R, given by Eqs. (2-5), (2-6), and (2-7), are plotted in Fig. 2-6, together with the -1/N(E/h) trajectory. The following system parameters are used:

$K_p = 1.65 \times 10^6$ $\qquad$ $K_R = 3.71 \times 10^5$

$K_I = 7.33 \times 10^5$ $\qquad$ $J_v = 41822$

Figure 2-6 shows that since the plot of $G_D(s)$ does not intersect the -1/N(E/h) trajectory in the finite domain, the quantizer Q_D will not cause any self-sustained oscillations in the LST system.

Both the curves for $G_T(s)$ and $G_R(s)$ intersect the -180-degree axis and the -1/N(E/h) trajectory at 25 db.

Thus,

$$20 \log_{10}|1/N(E/h)| = 25 \text{ db} \tag{2-26}$$

which gives

$$N(E/h) = 0.05012 \tag{2-27}$$

Figure 2-4 shows that for this value of N(E/h),

$$\frac{E}{h} \cong 0.5 \tag{2-28}$$

or

$$E \cong 0.5\, h \tag{2-29}$$

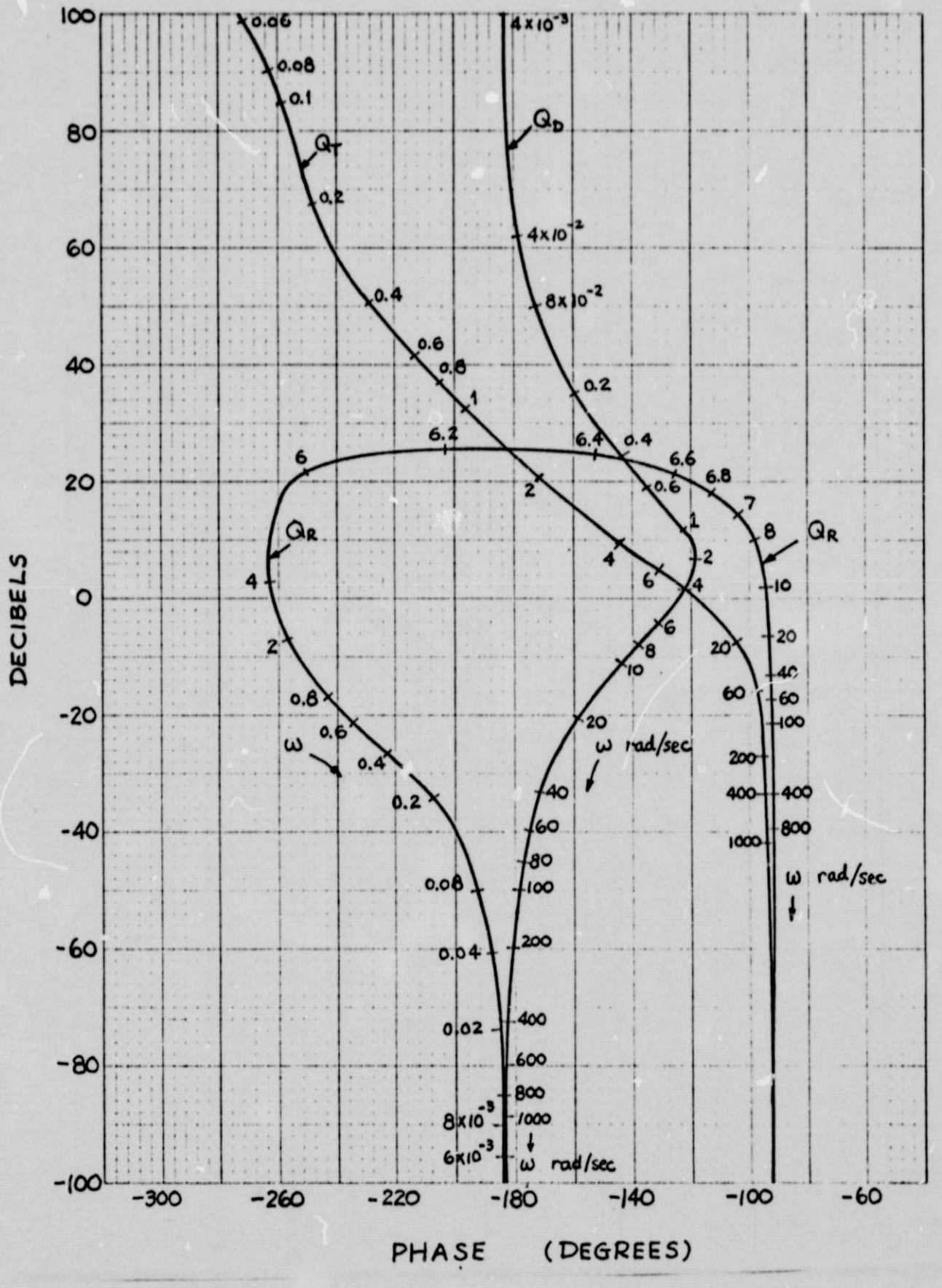

Figure 2-6. G(s) plots for the analog low-cost LST system with various quantizers.

This means that the quantizers Q_T and Q_R each independently may cause self-sustained oscillations to occur in the LST system. Furthermore, the self-sustained oscillations will have an amplitude equal to one-half the level of quantization h. Another point of interest is that the intersect between $G_T(s)$, $G_R(s)$, and $-1/N(E/h)$ corresponds to $n = 1$, so that the quantizers Q_T and Q_R are essentially acting as a simple relay with dead zone.

Figure 2-6 shows that the frequency of the oscillations caused by Q_T is 1.5 rad/sec, and that caused by Q_R is 6.3 rad/sec.

It is interesting to point out that the analysis in Chapter 1 shows that the displacement quantizer Q_D produces far greater quantization error than the torque and rate quantizers. However, the describing function analysis shows that Q_D does not cause self-sustained oscillations, whereas Q_T and Q_R may excite oscillations with amplitudes equal to one-half the level of quantization, h/2. All these factors must be taken into consideration when selecting the quantization level.

3. Stability of the Analog Low-Cost Large Space Telescope with Reaction Wheel Friction Nonlinearity

3-1. Introduction

The objective of this chapter is to conduct an investigation on the pointing stability of the analog model of the low-cost Large Space Telescope (LST) System with the reaction wheel frictional nonlinearity.

Although the LST system is digital, the stability study on the analog model will establish a limiting case when the sampling period becomes very small, thus providing a check on the results of the digital system.

The block diagram of the digital low-cost LST system, including the reaction wheel dynamics, is shown in Fig. 1-1. It has been shown in Section 1-1 that the dynamics of the LST system can be simplified. Figure 3-1 shows the block diagram of the simplified low-cost LST system with the reaction wheel nonlinearity.

The Δ of the system shown in Fig. 3-1 is

$$\Delta = 1 + K_R G_4 + G_1 G_4 G_5 + N G_6 G_7 \tag{3-1}$$

where N denotes the continuous-data describing function of the reaction wheel frictional nonlinearity.

Substitution of the expressions of G_1, G_4, G_5, G_6, and G_7 into Eq. (3-1), we have

$$\Delta = 1 + \frac{K_R}{J_v s} + \left(K_p + \frac{K_I}{s}\right)\frac{1}{J_v s^2} + N\,\frac{1}{J_{RW} s^2} \tag{3-2}$$

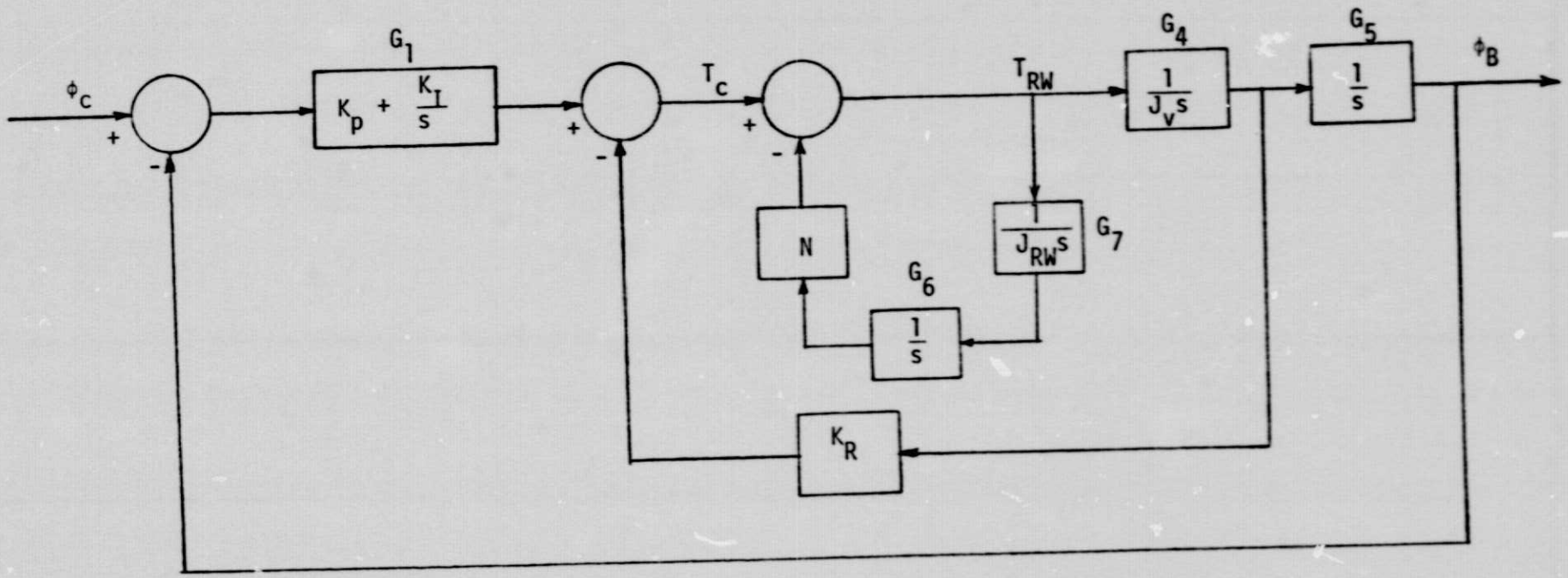

Figure 3-1. Simplified low-cost LST system with reaction wheel nonlinearity.

Setting Δ to zero, and rearranging Eq. (3-2), we get

$$J_v J_{RW} s^3 + J_{RW} K_R s^2 + J_{RW}(K_p s + K_I) + N J_v s = 0 \qquad (3\text{-}3)$$

which is the "characteristic equation" of the system.

3-2. Condition of Self-Sustained Oscillations in the Analog LST System with Reaction Wheel

It has been shown [1] that the nonlinear frictional characteristics of a reaction wheel can be described by the Dahl model. Therefore, the analog describing function of the CMG frictional nonlinearity derived in [2] can be directly utilized.

The equivalent transfer function that N sees is determined from Eq. (3-3) by dividing both sides of the equation by the terms that do not contain N. We have

$$1 + \frac{NJ_v s}{J_{RW}(J_v s^3 + K_R s^2 + K_p s + K_I)} = 0 \qquad (3\text{-}4)$$

Thus,

$$G_{eq}(s) = \frac{J_v s}{J_{RW}(J_v s^3 + K_R s^2 + K_p s + K_I)} \qquad (3\text{-}5)$$

The condition of self-sustained oscillation is investigated by plotting $G_{eq}(j\omega)$ and $-1/N$ in the magnitude (db) versus phase coordinates. Figure 3-2 shows the plot of $G_{eq}(j\omega)$ of the LST system with

$K_R = 3.71 \times 10^5$

$K_p = 1.65 \times 10^6$

$K_I = 7.33 \times 10^5$

$J_v = 41822$

$J_{RW} = 0.2$

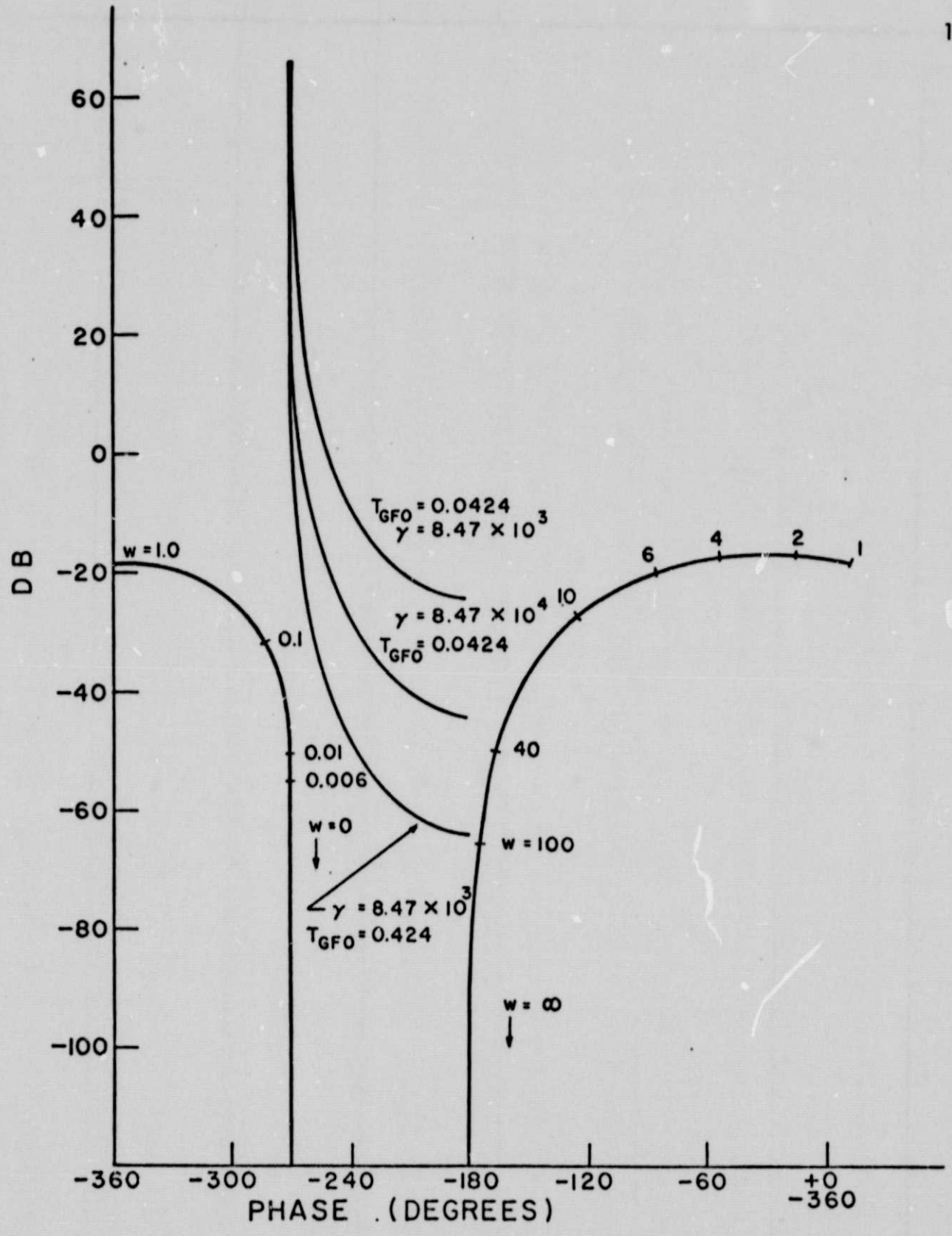

Figure 3-2. $G_{eq}(j\omega)$ and -1/N plots of analog LST with reaction wheel and frictional nonlinearity.

and the plots of -1/N with

(i) $\gamma = 8470$ $T_{GFO} = 0.0424$

(ii) $\gamma = 84700$ $T_{GFO} = 0.0424$

(iii) $\gamma = 8470$ $T_{GFO} = 0.424$

Since the $G_{eq}(j\omega)$ plot never enters the region bounded by -180° and -270° in which the plot of -1/N lies, the analog LST system will not have self-sustained oscillations, due to the reaction wheel frictional nonlinearity.

4. Stability of the Digital Low-Cost Large Space Telescope With Reaction Wheel Friction Nonlinearity

4-1. Introduction

In this chapter we shall investigate the condition of self-sustained oscillations of the digital low-cost LST system with reaction wheel friction nonlinearity.

The block diagram of the simplified LST system is shown in Fig. 4-1. The equations written for the outputs of the samplers are:

$$\Phi_e(z) = -G_A(z)\Phi_e(z) + N(z)G_B(z)\Theta_{RW}(z) \tag{4-1}$$

$$\Theta_{RW}(z) = G_c(z)\Phi_e(z) - N(z)G_D(z)\Theta_{RW}(z) \tag{4-2}$$

where $N(z)$ denotes the discrete describing function of the reaction wheel friction nonlinearity. Since the friction nonlinearity of the reaction wheel can be represented by the Dahl model, $N(z)$ is identical to the discrete describing function of the CMG nonlinearity [2].

The transfer functions in Eqs. (4-1) and (4-2) are

$$G_A(z) = \mathcal{Z}\left[\frac{G_{ho}G_1G_2G_3}{1 + K_RG_2}\right] \tag{4-3}$$

$$G_B(z) = \mathcal{Z}\left[\frac{G_{ho}G_2G_3}{1 + K_RG_2}\right] \tag{4-4}$$

$$G_c(z) = \mathcal{Z}\left[\frac{G_{ho}G_1G_4G_5}{1 + K_RG_2}\right] \tag{4-5}$$

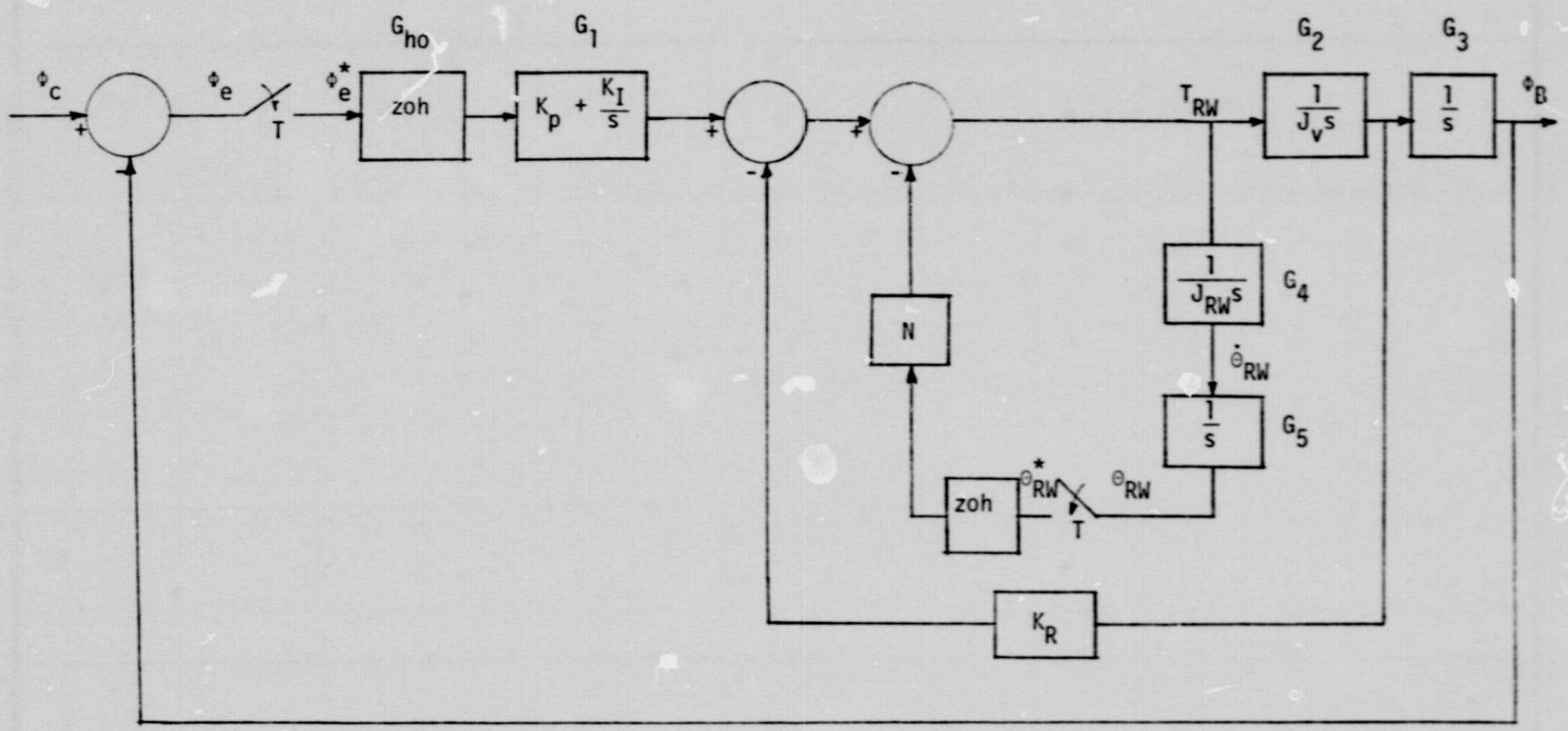

Figure 4-1. Block diagram of digital low-cost LST system with reaction wheel nonlinearity.

$$G_D(z) = \mathcal{Z}\left[\frac{G_{ho}G_4G_5}{1 + K_R G_2}\right] \tag{4-6}$$

The signal flow graph representing Eqs. (4-1) and (4-2) is shown in Fig. 4-2. The Δ of the system is obtained from Fig. 4-2,

$$\Delta = 1 + G_A(z) + N(z)[G_A(z)G_D(z) - G_B(z)\, G_c(z) + G_D(z)] \tag{4-7}$$

Setting Δ to zero, the last equation can be written in the form of

$$1 + N(z)G_{eq}(z) = 0 \tag{4-8}$$

where

$$G_{eq}(z) = \frac{G_A(z)G_D(z) - G_B(z)G_c(z) + G_D(z)}{1 + G_A(z)} \tag{4-9}$$

The individual transfer functions are evaluated as follows:

$$G_A(z) = (1 - z^{-1})\,\frac{1}{J_v}\,\mathcal{Z}\left[\frac{K_p}{s^2(s + a)} + \frac{K_I}{s^3(s + a)}\right]$$

$$= K_p G_B(z) + \frac{K_I}{J_v}\left[\frac{T^2(z + 1)}{2a(z - 1)^2} - \frac{T}{a^2(z - 1)} + \frac{1}{a^3} - \frac{z - 1}{a^3(z - e^{-aT})}\right] \tag{4-10}$$

$$a = K_R/J_v$$

$$G_B(z) = \frac{1}{K_R}\left[\frac{T}{z - 1} - \frac{1 - e^{-aT}}{a(z - e^{-aT})}\right] \tag{4-11}$$

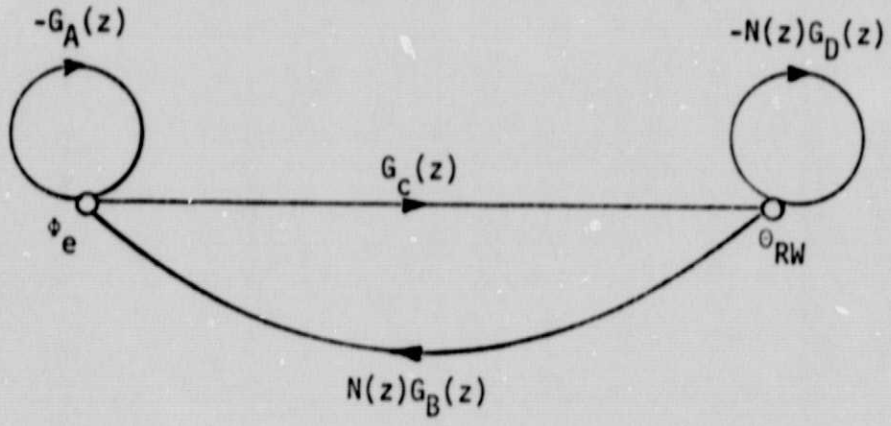

Figure 4-2. Signal flow graph.

$$G_C(z) = \frac{J_V}{J_{RW}} G_A(z) \qquad (4\text{-}12)$$

$$G_D(z) = \frac{J_V}{J_{RW}} G_B(z) \qquad (4\text{-}13)$$

4-2. Self-Sustained Oscillations in the Digital LST System With Reaction Wheel Nonlinearity

Figure 4-3 shows the plots of $G_{eq}(z)$ in Eq. (4-9) for various values of n with T as a parameter. The integer n and sampling period T are related to the frequency of oscillation by the following equation:

$$\omega_c = \frac{2\pi}{nT} \tag{4-14}$$

The following system parameters are used:

$K_p = 1.65 \times 10^6$ $\quad$ $K_R = 3.71 \times 10^5$

$K_I = 7.33 \times 10^5$ $\quad$ $J_v = 41822$

$J_{RW} = 0.2$

In Fig. 4-3 the curve for n = 2 extends up to approximately 30 db at T = 0.7 sec. Also, as n is increased the curves for $G_{eq}(z)$ approach the curve for $G_{eq}(s)$ presented in Fig. 3-2. The plots of $G_{eq}(z)$ together with the plots of -1/N(z) allow the study of self-sustained oscillations in the digital LST system.

Figures 4-4 through 4-6 show the plots for -1/N(z) for various n. In these plots $\gamma = 84700$ and $T_{GFO} = 0.424$. In all cases, the magnitude of the lowest point of the -1/N(z) curve as E approaches 0 is given by

$$\lim_{E \to 0} \frac{1}{|N(z)|} = \frac{1}{\gamma T_{GFO}^2} \tag{4-15}$$

With the given parameters this point is at -83.66 db. The curves for n = 2 are shown in Fig. 4-4 and consist of two straight lines at

$-180°$ (for $0 \leq \phi < \pi/2$) and $-360°$ (for $\pi/2 < \phi \leq \pi$). The plots for $n = 3$ and $n = 4$ are shown in Figs. 4-5 and 4-6, respectively. Several values of ϕ are plotted in each case to illustrate the effect of the phase of the input signal. It should be noted that for odd n the curves repeat every 180/n degrees starting from $\phi = 0$, and for even n the curves repeat every 360/n degrees starting from $\phi = 0$. As the input amplitude E goes to infinity, the curves also go to infinity and span a region 180/n degrees or 360/n degrees wide for odd or even n, respectively. This region is centered about the $-270°$ line. Thus, as n goes to infinity these curves approach the $-1/N$ curve of the continuous system shown in Fig. 3-2.

For stability analysis it is sufficient to consider only the bounds of the $-1/N(z)$ plot for a fixed n. Self-sustained oscillations can occur if the $G(z)$ curve corresponding to the same n intersects with the $F(z)$ plot. Figures 4-3 through 4-6 show that self-sustained oscillations can readily occur in this system with the choice of T determining the possible n values which can exist. As the critical regions for higher values than $n = 4$ can be easily visualized, it is apparent that this system will have self-sustained oscillations for integral values beyond $n = 4$. However, as n increases, the amplitude of oscillation decreases and the oscillation will eventually cease as T gets smaller and smaller and n gets larger and larger.

If γ and T_{GRO} are increased then the curves of $-1/N(z)$ move up with the end point shifting according to Eq. (4-15). Figures 4-7 through 4-9 show the plots of $-1/N(z)$ for $n = 2$, 3 and 4, respectively, with $\gamma = 8470$ and $T_{GFO} = 0.0424$. In this case the lowest point is at -23.66 db and

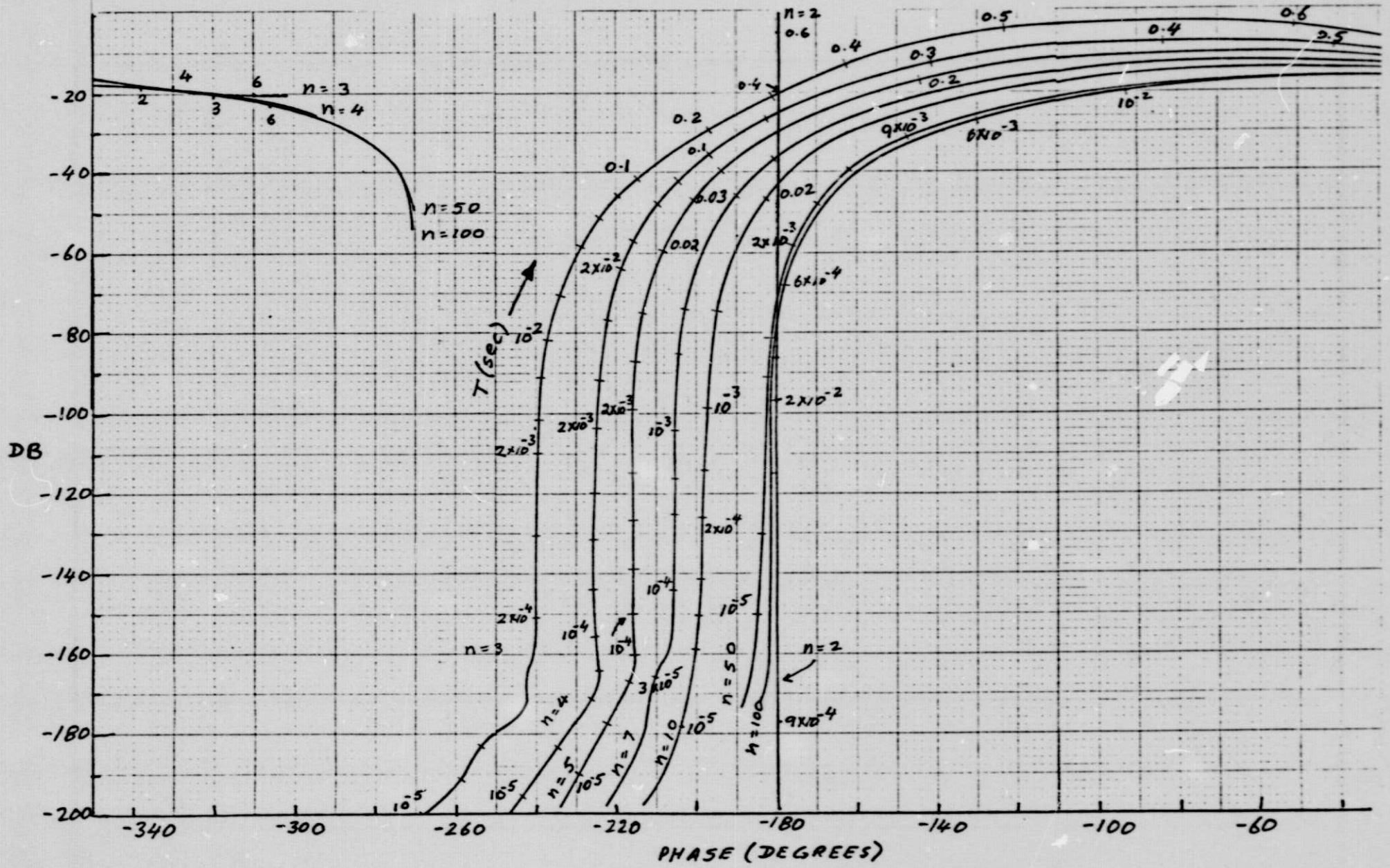

Figure 4-3. G(z) curves of the low-cost LST with frictional nonlinearity.

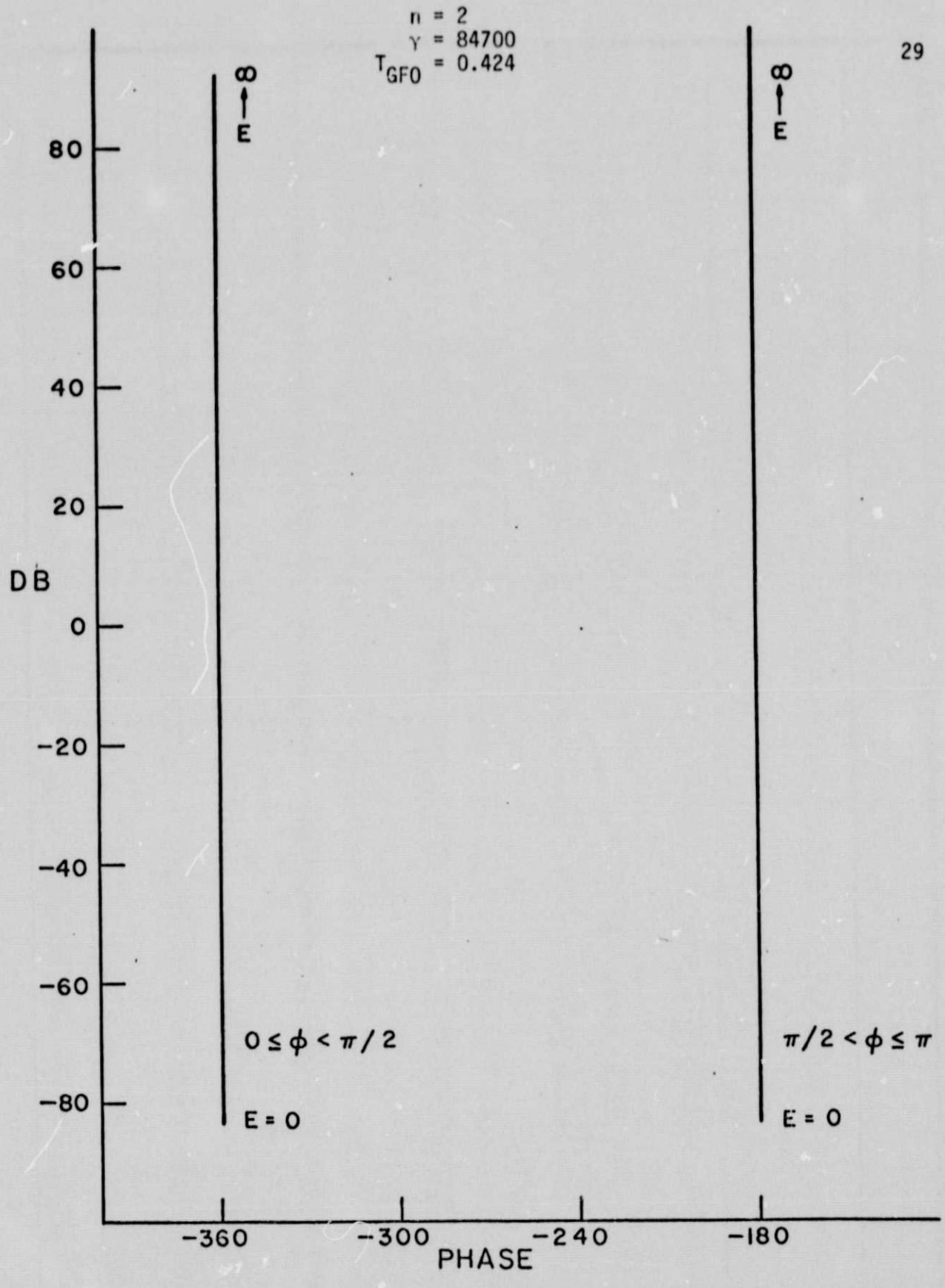

Figure 4-4. Discrete describing function for the frictional nonlinearity, n = 2.

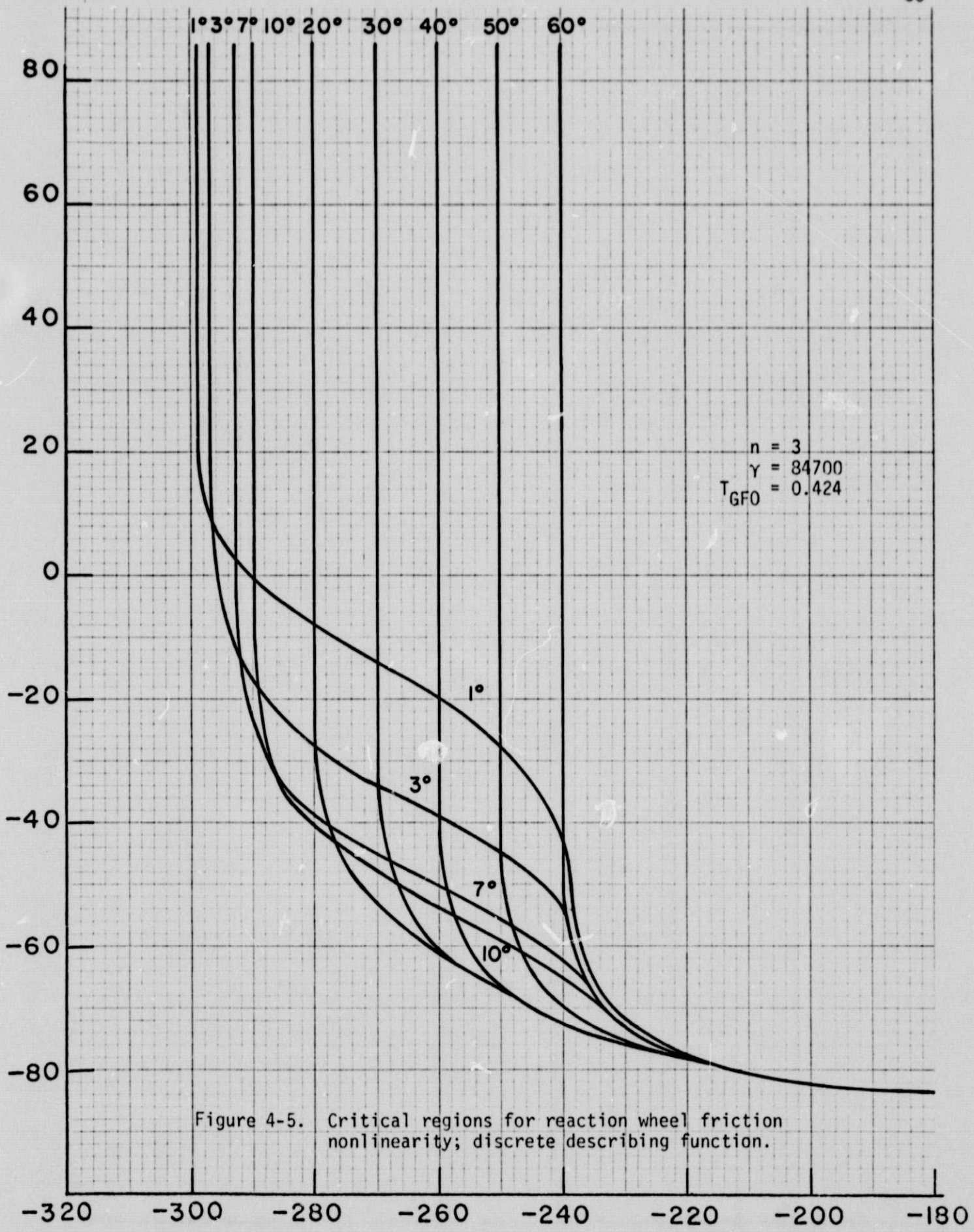

Figure 4-5. Critical regions for reaction wheel friction nonlinearity; discrete describing function.

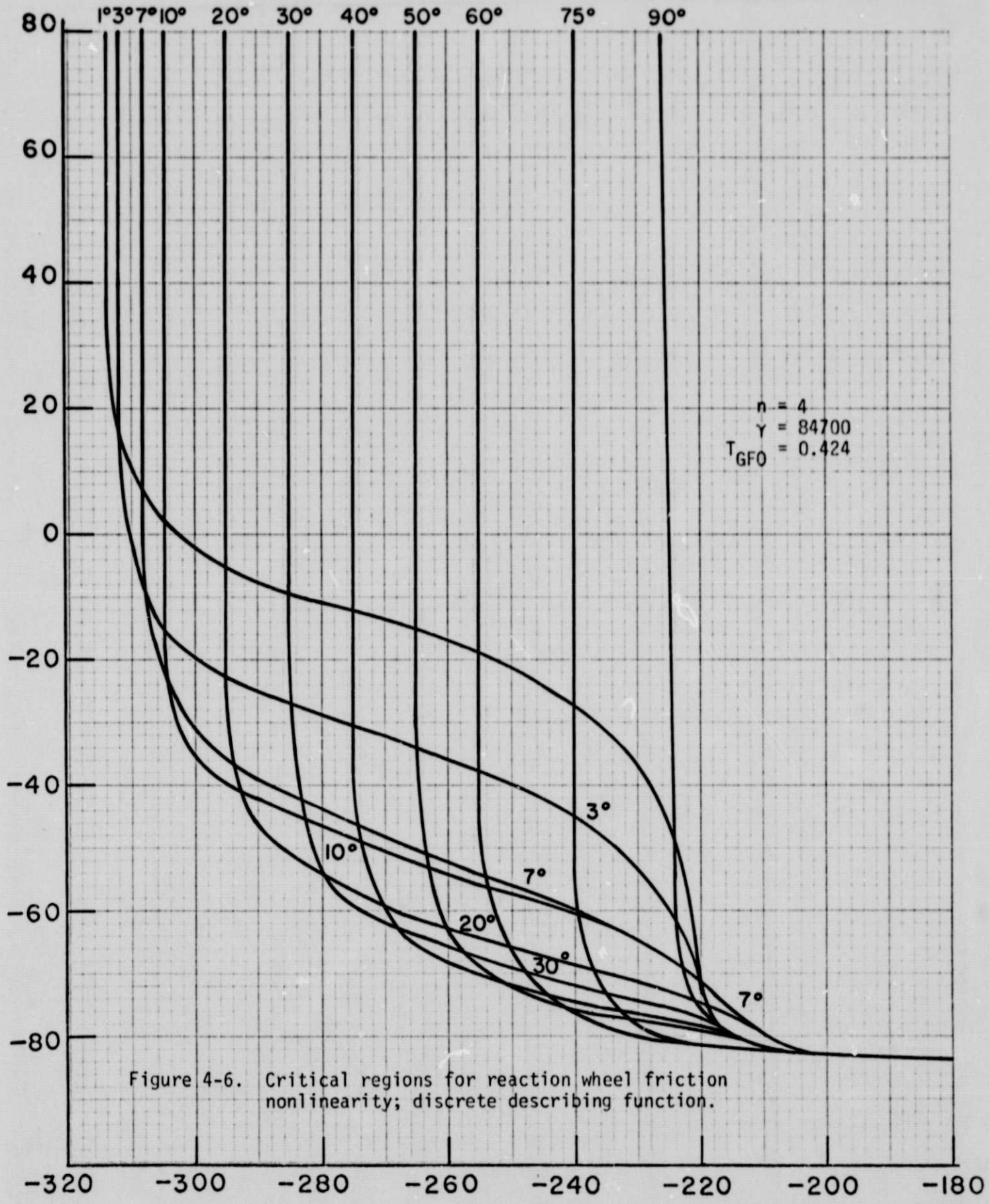

Figure 4-6. Critical regions for reaction wheel friction nonlinearity; discrete describing function.

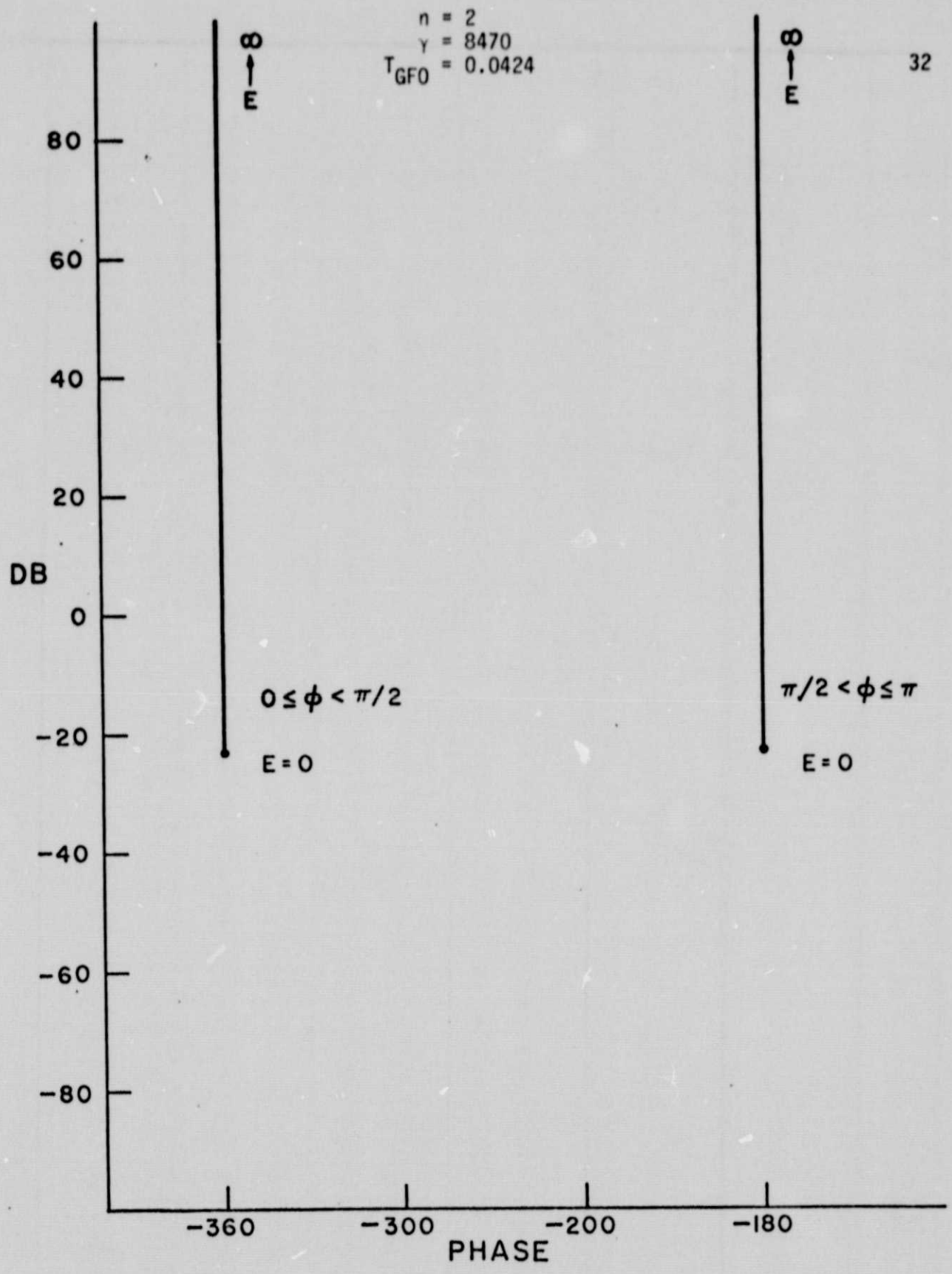

Figure 4-7. Discrete describing function for the frictional nonlinearity, n = 2.

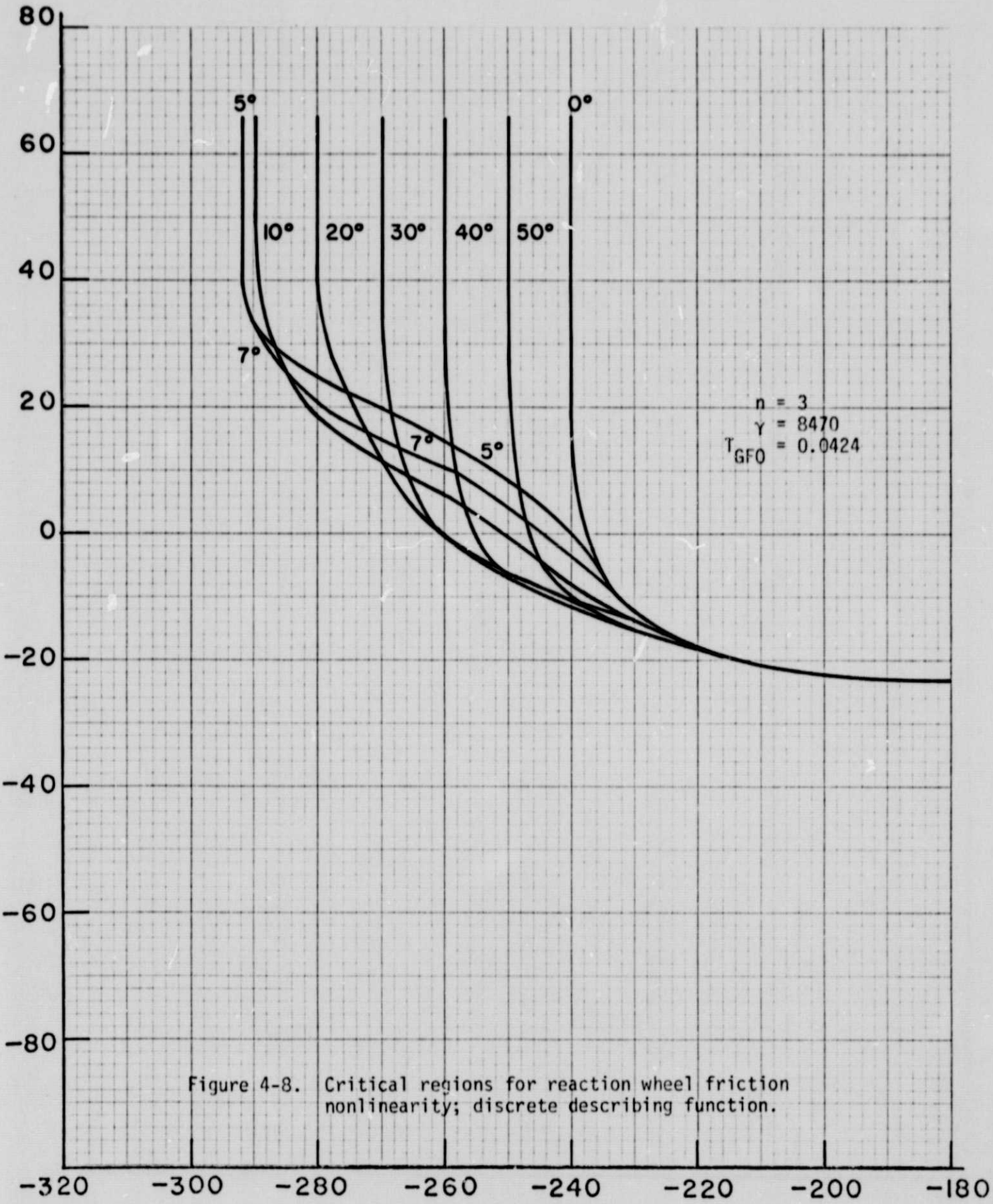

Figure 4-8. Critical regions for reaction wheel friction nonlinearity; discrete describing function.

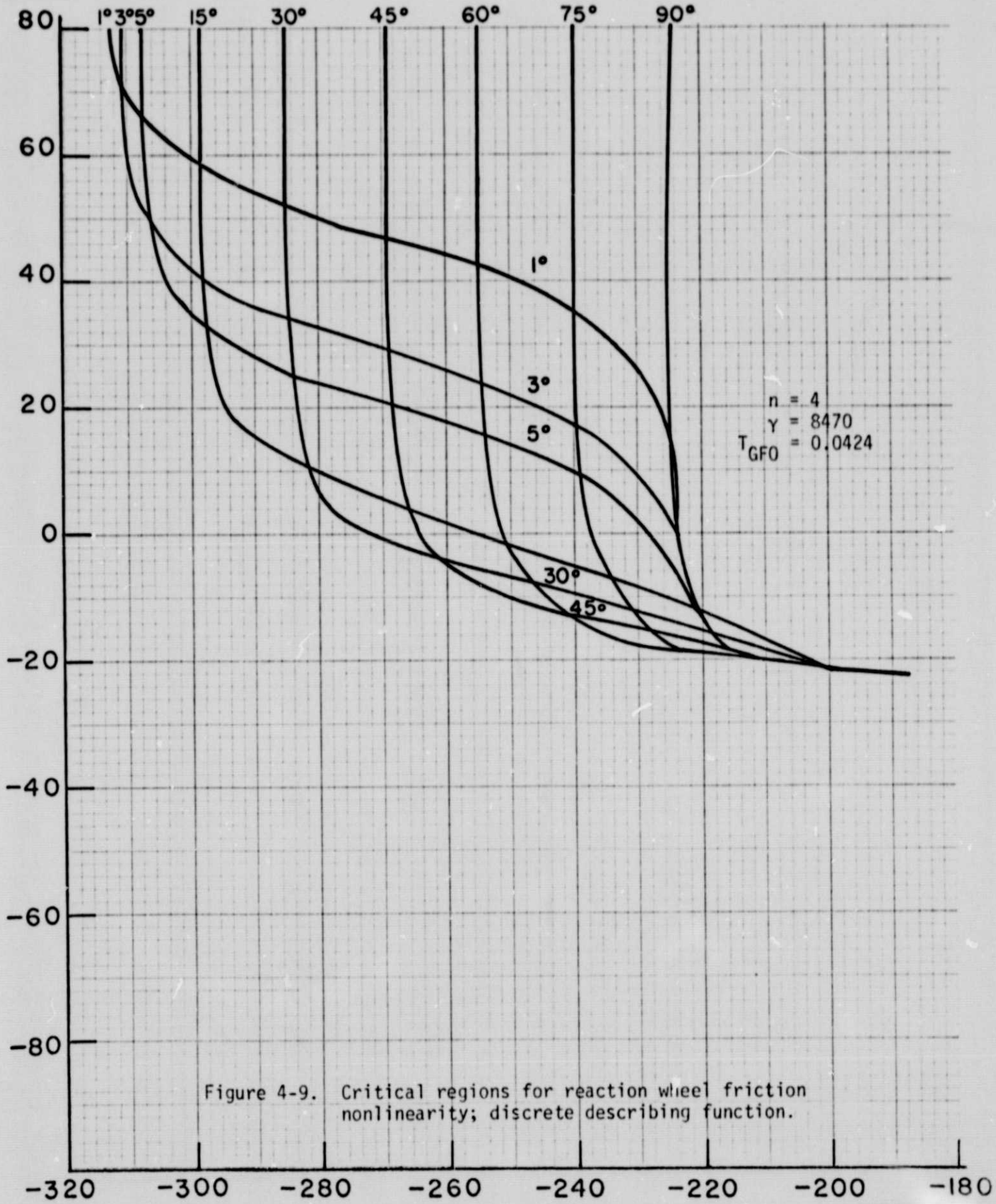

Figure 4-9. Critical regions for reaction wheel friction nonlinearity; discrete describing function.

self-sustained oscillations are possible only for n = 2 over a fixed small range of sampling periods. If T is chosen to exclude the critical region, self-sustained oscillations can be avoided.

REFERENCES

1. K. Frevert and R. Joyce, "Pointing Stability of A Fine Pointing Control System For A Low-Cost LST With A Reaction Wheel Model And Dahl Nonlinearity," Northrop Services, Inc., Memorandum No. 9250C-74-51, December 20, 1974.

2. B. C. Kuo and G. Singh, "Continuous And Discrete Describing Function Analysis of the LST System," Chapter 1, Final Report, IV-73, Systems Research Laboratory, January 1, 1974.

5. Discrete Describing Function of A Quantizer

5-1. Introduction

The effects of quantization and the study of quantization error conducted in Chapter 1 are all based on the assumption that the digital system with quantization is stable and free from sustained oscillations. Since a quantizer is a nonlinear element, it can cause self-sustained oscillations. In Chapter 2 the condition of self-sustained oscillations in the analog low-cost LST system with quantizer is studied by use of the continuous-data describing function. However, in reality, the low-cost LST system is a digital system. The interaction between the sampling operation and the quantizer will bring about phenomena which can be grossly different from that in an analog system. Therefore, it is essential that the discrete describing function (DDF) of a quantizer be derived. To the authors' knowledge the DDF of a quantizer has not been derived in the past.

Figure 5-1 shows the input-output characteristics of a quantizer. The input of the quantizer is denoted by $e^*(t)$, and the output by $y^*(t)$. It is assumed that the input of the quantizer is the output of an ideal sampler. Therefore, $e^*(t)$ and $y^*(t)$ are trains of impulses. Furthermore, it is assumed that the input to the sampler, $e(t)$, is a cosine wave, and thus the amplitude of $e^*(t)$ is modulated by a cosine wave; that is,

$$e(t) = E \cos (\omega t + \phi) \tag{5-1}$$

$$e^*(t) = E \sum_{k=0}^{\infty} \cos (k\omega T + \phi)\delta(t - kT) \tag{5-2}$$

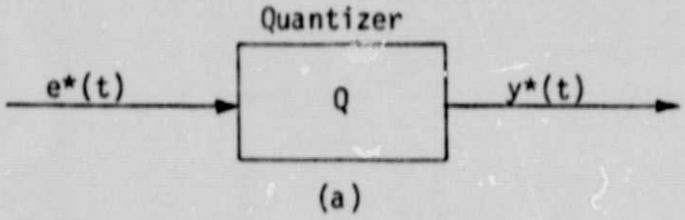

(a)

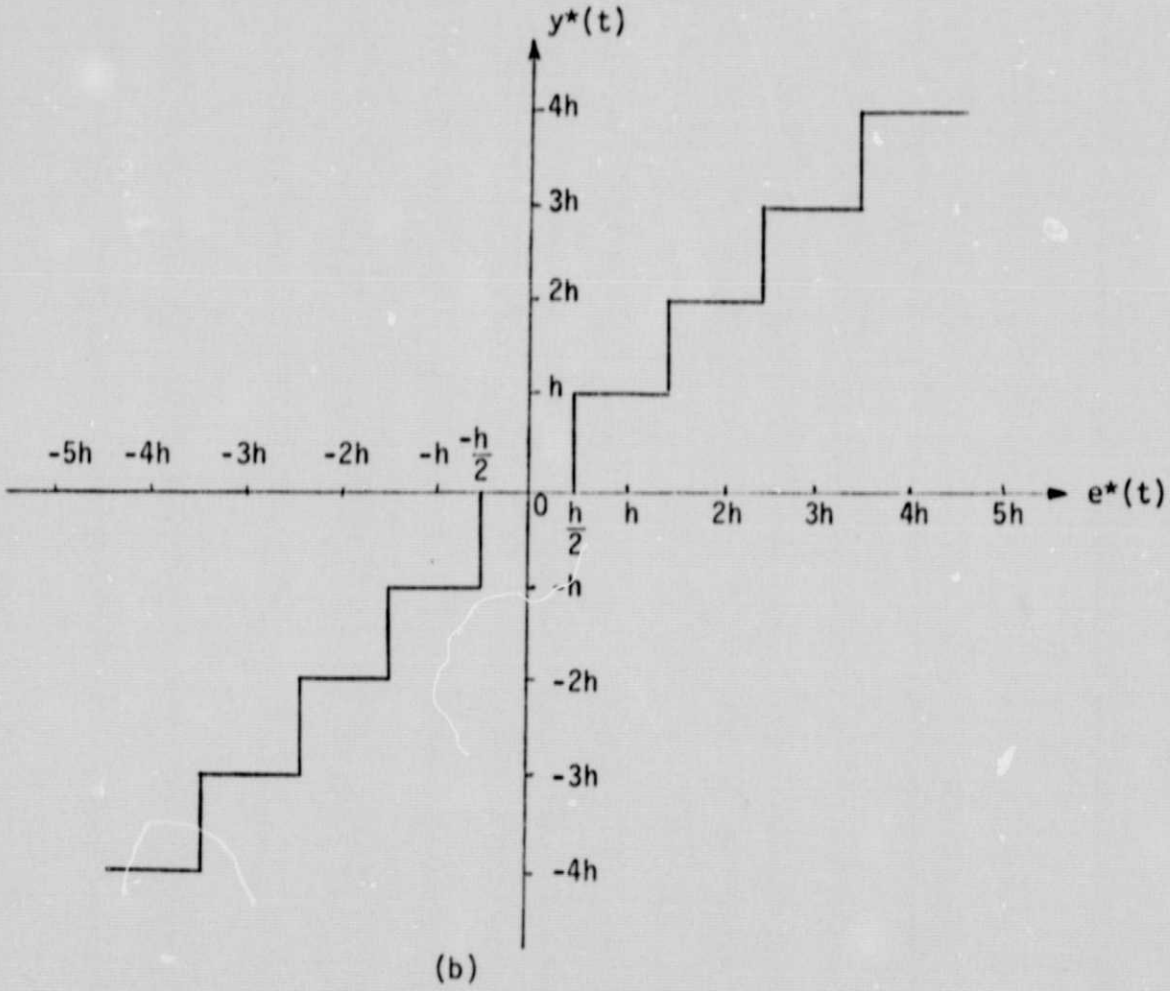

(b)

Figure 5-1. (a) Quantizer nonlinearity.

(b) Input-output relation of quantizer.

where E is a constant, ω is the frequency in radians per second, T is the sampling period in seconds, and $\delta(t)$ denotes the unit impulse function. The z-transform of $e^*(t)$ is

$$E(z) = \frac{Ez}{z^2 - 2z\cos\omega T + 1}[(z - \cos\omega T)\cos\phi - \sin\omega T \sin\phi] \tag{5-3}$$

The z-transform of $y^*(t)$ is denoted by $Y(z)$.

The discrete describing function of the quantizer nonlinearity is defined as

$$N(z) = \frac{Y(z)}{E(z)} \tag{5-4}$$

As in the case of the relay-type nonlinearity, we assume that because of the periodic nature of the sampler, $e^*(t)$ and $y^*(t)$ are all periodic functions of period nT, where n is a positive integer greater than or equal to two. Thus,

$$\omega = \frac{2\pi}{nT} \tag{5-5}$$

or

$$\omega T = \frac{2\pi}{n} \tag{5-6}$$

$n = 2, 3, 4, \ldots$.

The DDF N(z) is incorporated in the "characteristic equation" of the system,

$$1 + N(z)G_{eq}(z) = 0 \tag{5-7}$$

for the determination of the condition of self-sustained oscillations, where $G_{eq}(z)$ denotes the linear transfer function which the quantizer nonlinearity sees. Graphically, the condition of self-sustained oscillation characterized by the period nT is determined by the intersections of the $G_{eq}(z)$ trajectories with the critical regions of $-1/N(z)$, all for the same n. Therefore, the DDF problem involves the determination of the critical regions of $-1/N(z)$ for the quantizer for $n = 2, 3, \ldots$.

5-2. The DDF of A Quantizer for n = 2

In order to illustrate the derivation of the DDF of the quantizer nonlinearity, we shall first consider the case of n = 2; that is, the self-sustained oscillation is characterized by the period which is equal to twice the sampling period.

For this mode of oscillation, the waveforms of e(t), e*(t), and y*(t) are shown in Fig. 5-2.

For n = 2, Eq. (5-6) gives $\omega T = \pi$; Eq. (5-3) becomes

$$E(z) = \frac{Ez \cos \phi}{z + 1} \tag{5-8}$$

The z-transform of y*(t) is written

$$Y(z) = \frac{khz}{z + 1} \tag{5-9}$$

where k is a positive integer. In this case it is assumed that the value of E is constrained by the following equation:

$$\frac{(2k - 1)h}{2} < E \cos \phi < \frac{(2k + 1)h}{2} \tag{5-10}$$

Using Eqs. (5-8) and (5-9), we have

$$- \frac{1}{N(z)} = - \frac{E \cos \phi}{kh} \tag{5-11}$$

For a given set of values of k, h, and ϕ, the constraints on the values of E for n = 2 are

$$E_{max} = \frac{(2k + 1)h}{2 \cos \phi} \tag{5-12}$$

$$E_{min} = \frac{(2k - 1)h}{2 \cos \phi} \tag{5-13}$$

Substituting E_{max} and E_{min} into Eq. (5-11), we have

$$- \frac{1}{N(z)}\bigg|_{max}(k) = - \frac{(2k + 1)}{2k} \tag{5-14}$$

$$- \frac{1}{N(z)}\bigg|_{min}(k) = - \frac{(2k - 1)}{2k} \tag{5-15}$$

The last two equations indicate that the critical region for $-1/N(z)$ for $n = 2$ is the line which extends from $-(2k - 1)/2k$ to $-(2k + 1)/2k$ on the negative real axis in the polar coordinates.

It can be shown that

$$\frac{1}{N(z)}\bigg|_{max}(k+1) < \frac{1}{N(z)}\bigg|_{max}(k) \tag{5-16}$$

Since

$$\frac{1}{N(z)}\bigg|_{max}(k+1) = \frac{2(k + 1) + 1}{2(k + 1)} = 1 + \frac{1}{2(k + 1)} \tag{5-17}$$

and

$$\frac{1}{N(z)}\bigg|_{max}(k) = \frac{2k + 1}{2k} = 1 + \frac{1}{2k} \tag{5-18}$$

thus, Eq. (5-16) is verified.

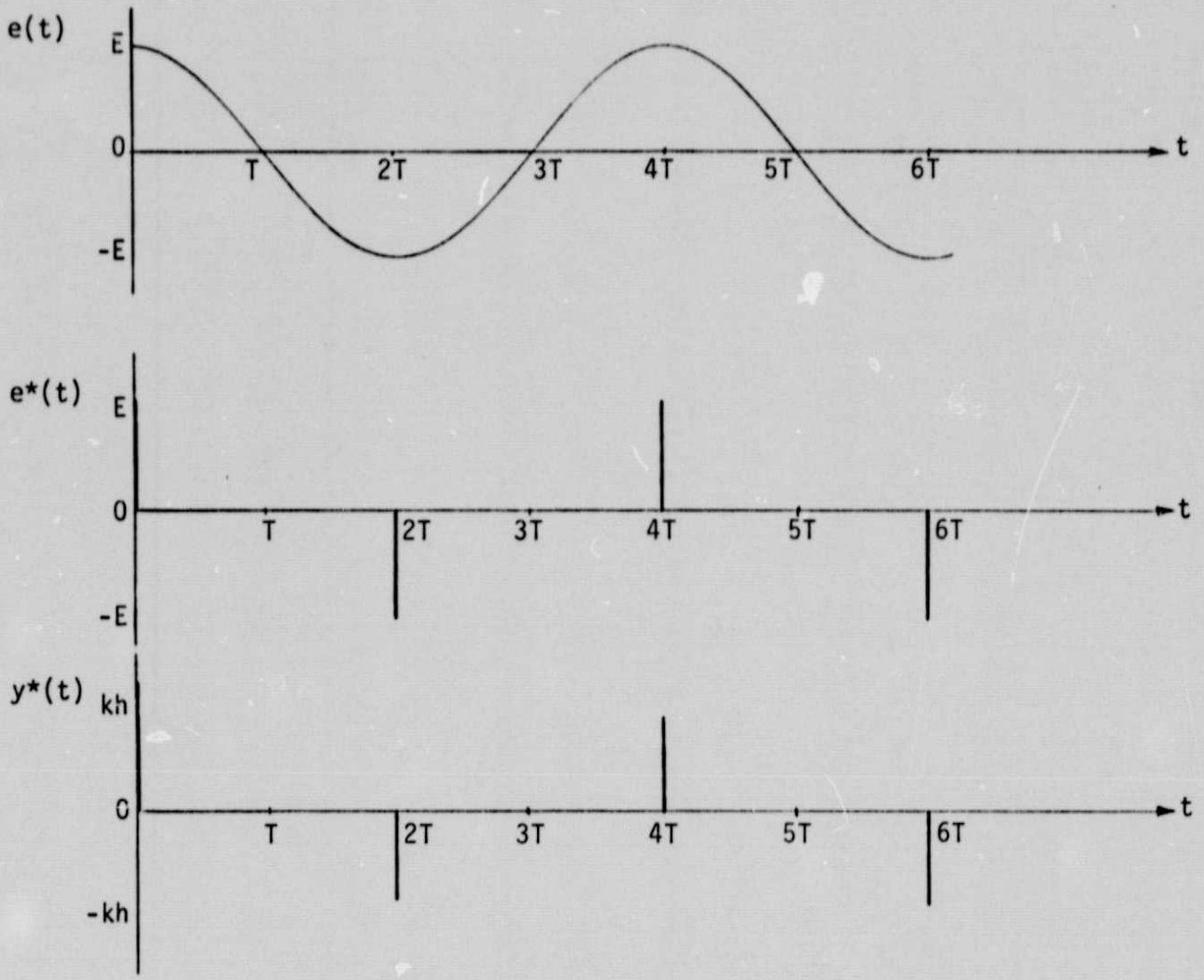

Figure 5-2. Waveforms for n = 2.

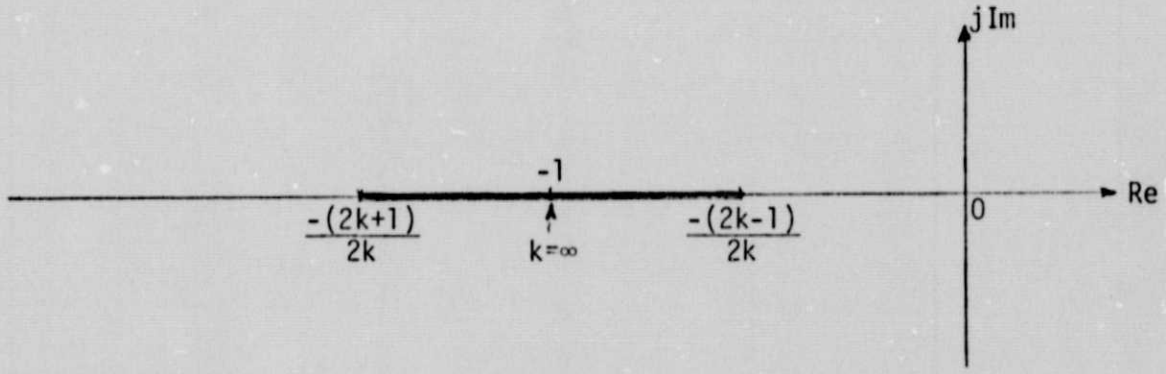

Figure 5-3. Critical region of -1/N(z) for quantizer for n = 2.

Similarly, using Eq. (5-15) we can show that, in general,

$$\left.\frac{1}{N(z)}\right|_{min}(k+1) > \left.\frac{1}{N(z)}\right|_{min}(k) \tag{5-19}$$

Thus, let S(k) be the set which is bounded by

$$-\left.\frac{1}{N(z)}\right|_{max}(k) \quad \text{and} \quad -\left.\frac{1}{N(z)}\right|_{min}(k) \quad ,$$

and S(k+1) be the set which is bounded by

$$-\left.\frac{1}{N(z)}\right|_{max}(k+1) \quad \text{and} \quad -\left.\frac{1}{N(z)}\right|_{min}(k+1) \quad ,$$

then

$$S(k+1) \subset S(k) \tag{5-20}$$

for k = 1, 2, 3, ...

Equations (5-14) and (5-15) also show that

$$\lim_{k\to o}\left[-\left.\frac{1}{N(z)}\right|_{max}(k)\right] = \lim_{k\to o}\left[-\left.\frac{1}{N(z)}\right|_{min}(k)\right] = -1 \tag{5-21}$$

This result implies that as the number of quantization levels increases, the quantizer characteristics approach a linear gain, and the critical region reduces to the (-1, j0) point in the complex plane.

The critical region for n = 2 is shown in Fig. 5-3.

5-3. The DDF of A Quantizer for n = 4

Before embarking on the derivations of general expressions of $-1/N(z)$ for all $n > 2$, the case for $n = 4$ will be considered as an illustrative example.

For $n = 4$, the input pulse train of the quantizer can assume a maximum of two different pulse amplitudes, k_0 and k_1. The mode of oscillation is thus characterized by $\Delta = (k_0, k_1)$, where k_0 and k_1 are positive integers. Figure 5-4 illustrates the input and the output of the sampler when the former is shifted through 360 degrees. It is observed from these waveforms, as well as will be verified later by equations, that the critical region for $n = 4$ repeats every 90 degrees for ϕ, so that only the range for $-45° \leq \phi \leq 45°$ needs be considered.

For $n = 4$, $\cos \omega T = \cos 90° = 0$, $z = j$. Thus, Eq. (5-3) becomes

$$E(z) = \frac{Ez}{z^2 + 1} (z \cos \phi - \sin \phi) \tag{5-22}$$

With reference to Fig. 5-4, the expressions of the input to the quantizer for the various ranges of ϕ are written as follows:

$$-90° \leq \phi \leq 0° \qquad Y(z) = \frac{h(k_0 z + k_1)z}{z^2 + 1} \tag{5-23}$$

$$-180° \leq \phi \leq -90° \qquad Y(z) = \frac{h(-k_0 z + k_1)z}{z^2 + 1} \tag{5-24}$$

$$0° \leq \phi \leq 90° \qquad Y(z) = \frac{h(k_0 z - k_1)z}{z^2 + 1} \tag{5-25}$$

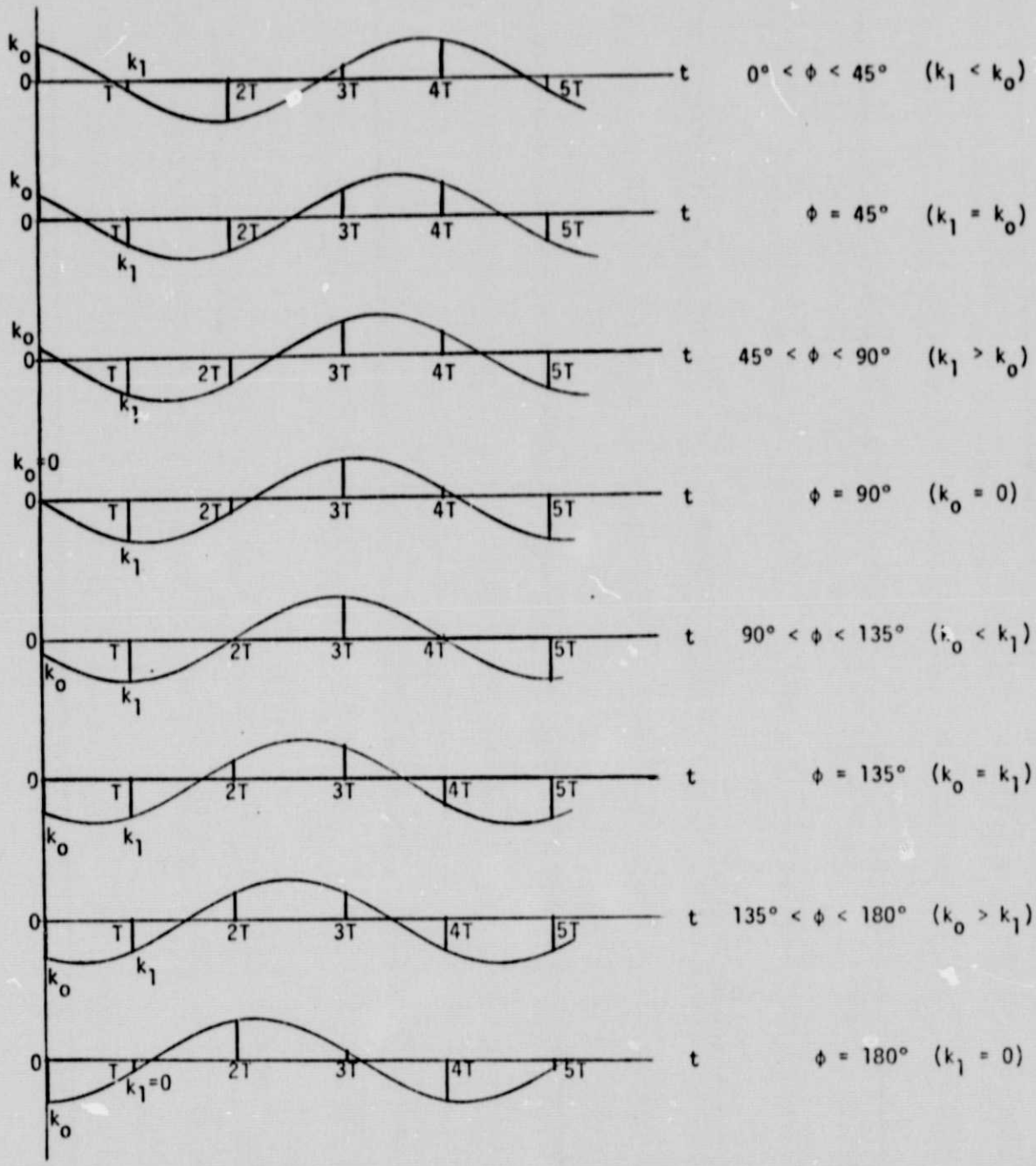

Figure 5-4. Input and output signal waveforms of sampler preceding the quantizer as ϕ varies through 360°.

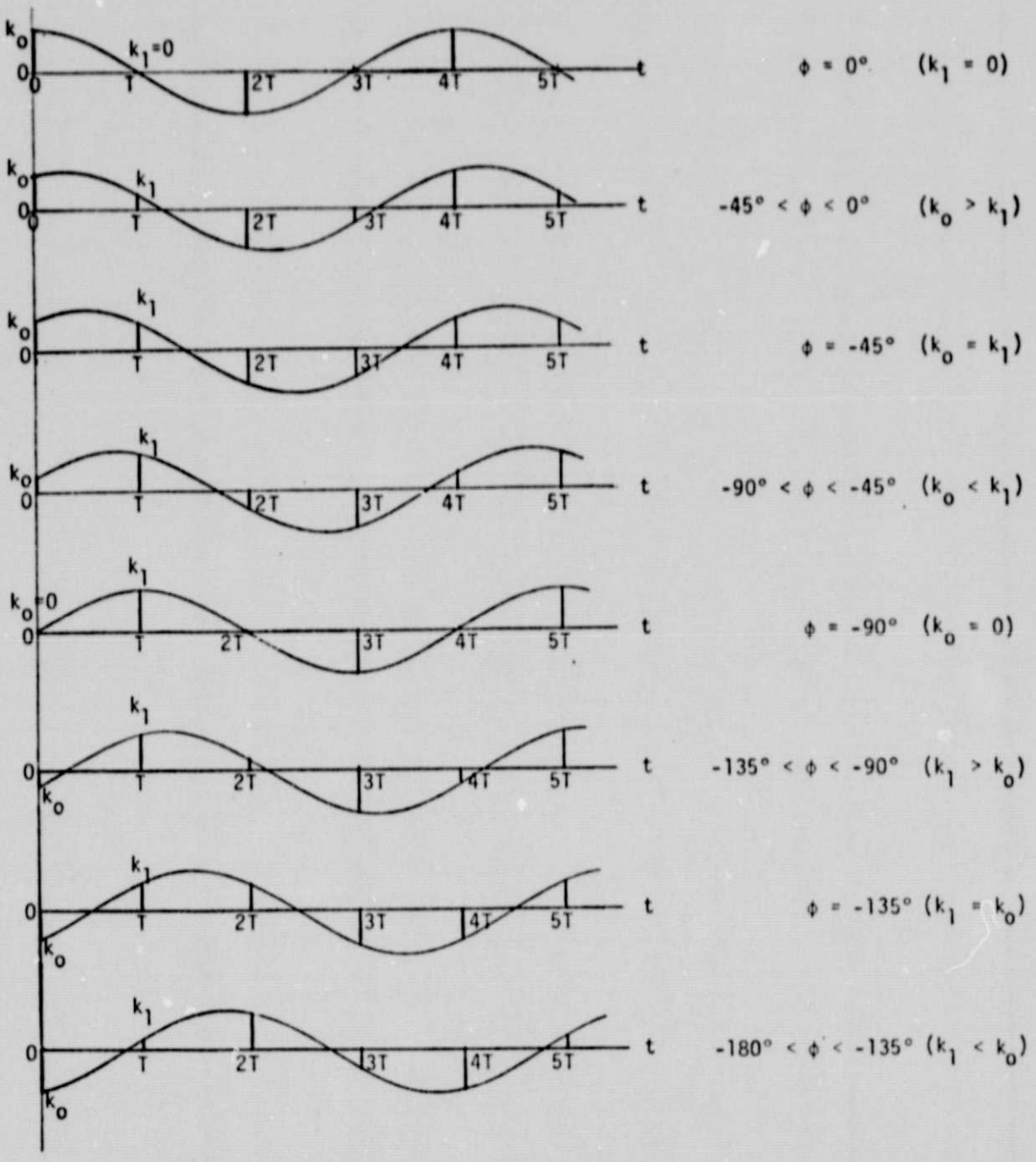

Figure 5-4. Input and output signal waveforms of sampler preceding the quantizer as ϕ varies through 360°.

$$90° \leq \phi \leq 180° \qquad Y(z) = \frac{h(-k_o z - k_1)z}{z^2 + 1} \tag{5-26}$$

The constraints on the magnitude of E over these ranges of ϕ are tabulated as follows:

$$\frac{(2k_o - 1)h}{2} \leq |E \cos \phi| \leq \frac{(2k_o + 1)h}{2} \tag{5-27}$$

and

$$\frac{(2k_1 - 1)h}{2} \leq |E \sin \phi| \leq \frac{(2k_1 + 1)h}{2} \tag{5-28}$$

These inequality conditions lead to maximum and minimum bounds on E. When these E_{max} and E_{min} are substituted into

$$-\frac{1}{N(z)} = -\frac{E(z)}{Y(z)} \tag{5-29}$$

and along with Eqs. (5-23) through (5-26), the equations that define the boundaries of the critical regions are obtained as

$$-\frac{1}{N(z)}\bigg|_{max} \qquad \text{and} \qquad -\frac{1}{N(z)}\bigg|_{min}$$

For instance, for $-90° \leq \phi \leq 0°$, from Eq. (5-27),

$$E_{min\,1} = \frac{(2k_o - 1)h}{2 \cos \phi} \tag{5-30}$$

Using Eqs. (5-22), (5-23), and (5-29), we have

$$-\left.\frac{1}{N(z)}\right|_{\min 1} = \frac{2k_o - 1}{2(k_o j + k_1)}(\tan\phi - j) \tag{5-31}$$

Rationalizing the last equation, we have

$$-\left.\frac{1}{N(z)}\right|_{\min 1} = \frac{2k_o - 1}{2(k_o^2 + k_1^2)}[(k_1 \tan\phi - k_o) + j(-k_o \tan\phi - k_1)] \tag{5-32}$$

Let

$$-\left.\frac{1}{N(z)}\right|_{\min 1} = R + jI \tag{5-33}$$

where

$$R = \frac{2k_o - 1}{2(k_o^2 + k_1^2)}(k_1 \tan\phi - k_o) \tag{5-34}$$

$$I = \frac{2k_o - 1}{2(k_o^2 + k_1^2)}(-k_o \tan\phi - k_1) \tag{5-35}$$

Then, solving for $\tan\phi$ from Eq. (5-34) gives

$$\tan\phi = \frac{R + k_o C}{k_1 C} \tag{5-36}$$

where

$$C = \frac{2k_o - 1}{2(k_o^2 + k_1^2)} \tag{5-37}$$

Substitution of Eq. (5-36) into Eq. (5-35) yields after simplification,

$$I = -\frac{k_o}{k_1} R - \frac{2k_o - 1}{2k_1} \tag{5-38}$$

which is the equation of a straight line in the complex $-1/N(z)$ domain.

Similarly, from Eq. (5-27),

$$E_{max\,1} = \frac{(2k_o + 1)h}{2\cos\phi} \qquad -90° \leq \phi \leq 0° \tag{5-39}$$

Following through the same procedure as described above, we have

$$-\frac{1}{N(z)}\bigg|_{max\,1} = \frac{2k_o + 1}{2(k_o j + k_1)}(\tan\phi - j) \tag{5-40}$$

which is represented by a straight line with the equation

$$I = -\frac{k_o}{k_1} R - \frac{2k_o + 1}{2k_1} \tag{5-41}$$

The boundaries for $-1/N(z)$ when the constraint equation of Eq. (5-28) is used are denoted as

$$-\frac{1}{N(z)}\bigg|_{max\,2} \qquad \text{and} \qquad -\frac{1}{N(z)}\bigg|_{min\,2}$$

The equations which define the boundaries of $-1/N(z)$ for the entire range of ϕ are tabulated below:

$-90° \leq \phi \leq 0°$	$I = -\frac{k_o}{k_1} R - \frac{2k_o - 1}{2k_1}$	(min 1)
$90° \leq \phi \leq 180°$		

$$I = -\frac{k_o}{k_1} R - \frac{2k_o + 1}{2k_1} \qquad \text{(max 1)}$$

$$I = \frac{k_1}{k_o} R + \frac{2k_1 - 1}{2k_o} \qquad \text{(min 2)}$$

$$I = \frac{k_1}{k_o} R + \frac{2k_1 + 1}{2k_o} \qquad \text{(max 2)} \qquad (5\text{-}42)$$

$-180° \leq \phi \leq -90°$

$0° \leq \phi \leq 90°$

$$I = \frac{k_o}{k_1} R + \frac{2k_o - 1}{2k_1} \qquad \text{(min 1)}$$

$$I = \frac{k_o}{k_1} R + \frac{2k_o + 1}{2k_1} \qquad \text{(max 1)}$$

$$I = -\frac{k_1}{k_o} R - \frac{2k_1 - 1}{2k_o} \qquad \text{(min 2)}$$

$$I = -\frac{k_1}{k_o} R - \frac{2k_1 + 1}{2k_o} \qquad \text{(max 2)} \qquad (5\text{-}43)$$

These equations show that for the oscillatory mode of n = 4 and $\Delta = (k_o, k_1)$, the critical regions are bounded by straight lines, and that it is sufficient to consider the range of $-90° \leq \phi \leq 90°$. However, Fig. 5-4 shows that $k_o \geq k_1$ for $-45° \leq \phi \leq 45°$ and $k_o \leq k_1$ for $45° \leq |\phi| \leq 90°$, thus, the critical regions for modes $\Delta = (k_o, k_1)$ and $\Delta = (k_1, k_o)$ are identical. It is necessary only to consider the range of ϕ from -45° to +45°. In general, one does not have to use the constraints on ϕ, as the intersects of the eight equations in Eqs. (5-42) and (5-43) will naturally define the critical region.

Modes $\Delta = (k_o, 0)$ *and* $\Delta = (0, k_1)$

Figure 5-4 shows that when $\phi = 0°$ or $180°$, $k_1 = 0$, and the mode is described as $\Delta = (k_o, 0)$. Similarly, when $\phi = \pm 90°$, the mode is $\Delta = (0, k_1)$.

For the mode $\Delta = (k_o, 0)$, Eqs. (5-42) and (5-43) are reduced to

$$R = -\frac{2k_o - 1}{2k_o} \qquad \text{(min 1)}$$

$$R = -\frac{2k_o + 1}{2k_o} \qquad \text{(max 1)}$$

$$I = -\frac{1}{2k_o} \qquad \text{(min 2)}$$

$$I = \frac{1}{2k_o} \qquad \text{(max 2)} \qquad (5\text{-}44)$$

These four lines define a square as shown in Fig. 5-5.

For the mode $\Delta = (0, k_1)$, it is simple to show that the critical region is described by equations of the same form of Eq. (5-44) with k_o replaced by k_1. Therefore, the square region shown in Fig. 5-5 is also for the mode $\Delta = (0, k_1)$ with k_o replaced by k_1.

Mode $\Delta = (k_o, k_1)$, $k_o = k_1$

When $\phi = \pm 45°, \pm 135°$, $k_o = k_1$, as shown in Fig. 5-4. The critical region is now described by the following four equations:

$$I = -R - \frac{2k_o - 1}{2k_o}$$

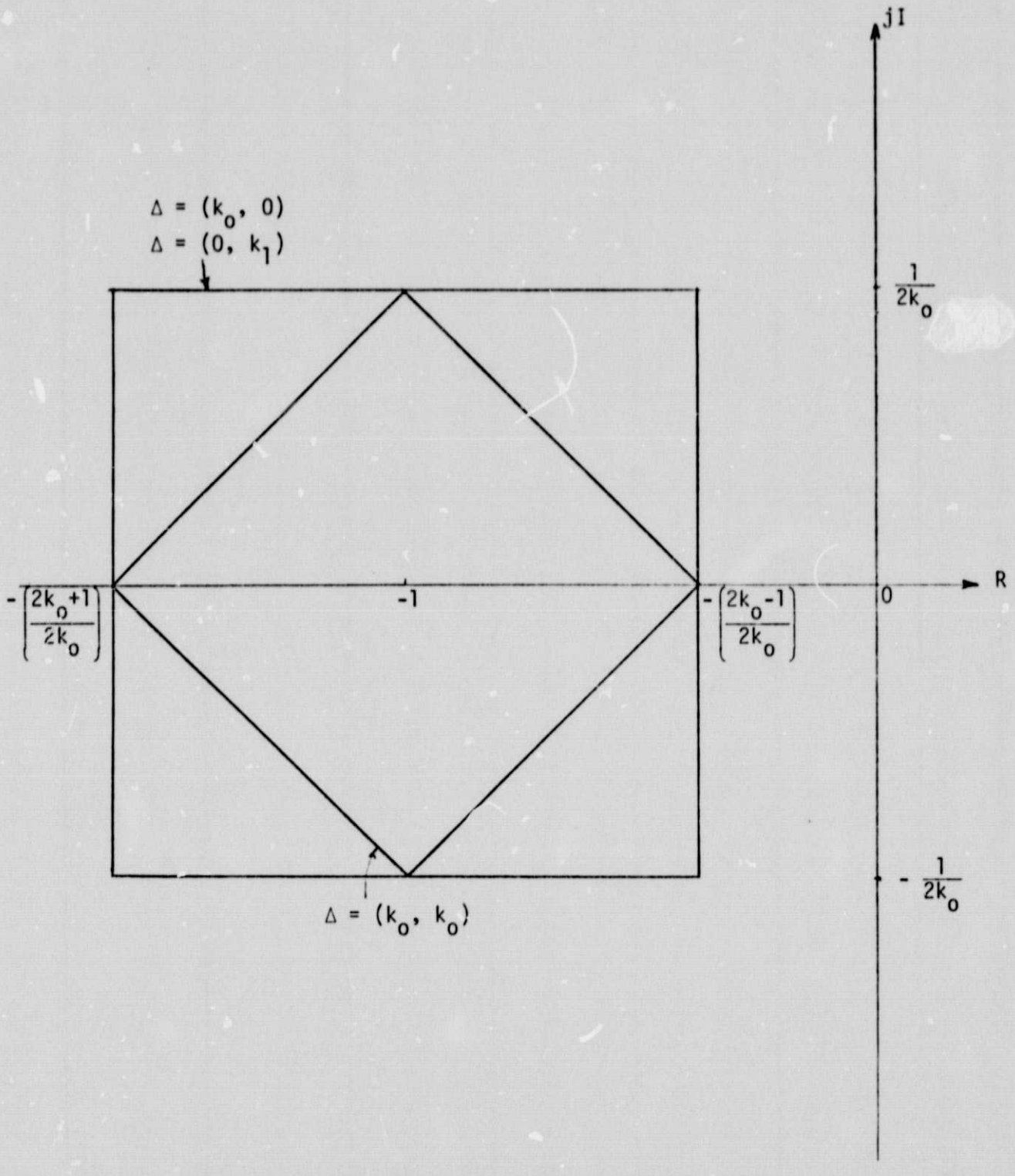

Figure 5-5. Critical regions of $\Delta = (k_o, 0)$, $(0, k_1)$, and (k_o, k_o).

$$I = -R - \frac{2k_o + 1}{2k_o}$$

$$I = R + \frac{2k_o - 1}{2k_o}$$

$$I = R + \frac{2k_o + 1}{2k_o} \qquad (5\text{-}45)$$

The critical region is again a square, as shown in Fig. 5-5.

In general, the critical region for the mode $\Delta = (k_o, k_1)$ is defined by the intersects of the eight equations in Eqs. (5-42) and (5-43). As an illustration, Fig. 5-6 shows the critical region for $\Delta = (2, 1)$ which is also for $\Delta = (1, 2)$. Notice that this critical region is bounded by that of $\Delta = (2, 0)$ or $\Delta = (0, 2)$.

(1) I = -2R - 3/2
(2) I = -2R - 5/2
(3) I = 2R + 3/2
(4) I = 2R + 5/2
(5) I = R/2 + 1/4
(6) I = R/2 + 3/4
(7) I = -R/2 - 1/4
(8) I = -R/2 - 3/4

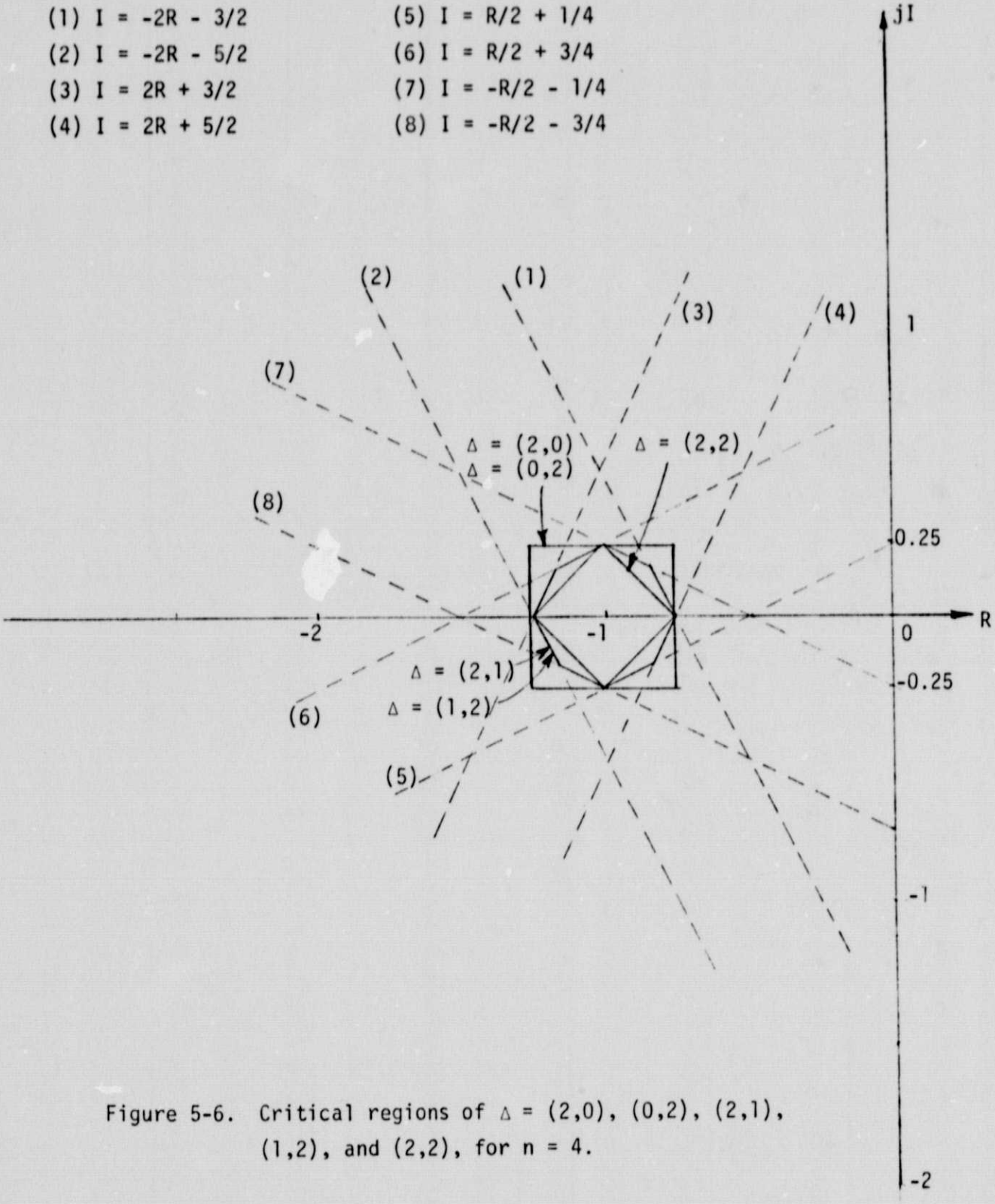

Figure 5-6. Critical regions of Δ = (2,0), (0,2), (2,1), (1,2), and (2,2), for n = 4.